Atmospheric
Measurement
Techniques

Next-generation ice-nucleating particle sampling on board aircraft: characterization of the High-volume flow aERosol particle filter sAmpler (HERA)

Sarah Grawe, Conrad Jentzsch, Jonas Schaefer, Heike Wex, Stephan Mertes, and Frank Stratmann

Atmospheric Microphysics, Leibniz Institute for Tropospheric Research, Leipzig, Germany

Correspondence: Sarah Grawe (grawe@tropos.de)

Abstract. Atmospheric ice-nucleating particle (INP) concentration data from the free troposphere are sparse but urgently needed to understand vertical transport processes of INPs and their influence on cloud formation and properties. Here, we introduce the new High-volume flow aERosol particle filter sAmpler (HERA) which was specially developed for installation on research aircraft and subsequent offline INP analysis. HERA is a modular system consisting of a sampling unit and a powerful pump unit, and it has several features which were integrated specifically for INP sampling. Firstly, the pump unit enables sampling at flow rates exceeding $100\,\mathrm{L\,min^{-1}}$, which is well above typical flow rates of aircraft INP sampling systems described in the literature ($\sim 10\,\mathrm{L\,min^{-1}}$). Consequently, required sampling times to capture rare, high-temperature INPs ($\geq -15\,^\circ\mathrm{C}$) are reduced in comparison to other systems, and potential source regions of INPs can be confined more precisely. Secondly, the sampling unit is designed as a seven-way valve, enabling switching between six filter holders and a bypass with one filter being sampled at a time. In contrast to other aircraft INP sampling systems, the valve position is remote-controlled via software so that manual filter changes during flight are eliminated and the potential for sample contamination is decreased. This design is compatible with a high degree of automation, i.e., triggering filter changes depending on parameters like flight altitude, geographical location, temperature, or time. In addition to presenting the design and principle of operation of HERA, this paper describes laboratory characterization experiments with size-selected test substances, i.e., SNOMAX® and Arizona Test Dust. The particles were sampled on filters with HERA, varying either particle diameter (300 to 800 nm) or flow rate (10 to $100\,\mathrm{L\,min^{-1}}$) between experiments. The subsequent offline INP analysis showed good agreement with literature data and comparable sampling efficiencies for all investigated particle sizes and flow rates. Furthermore, the collection efficiency of atmospheric INPs in HERA was compared to a straightforward filter sampler and good agreement was found. Finally, results from the first campaign of HERA on the High Altitude and LOng range research aircraft (HALO) demonstrate the functionality of the new system in the context of aircraft application.

1 Introduction

Ice-nucleating particles (INPs) have been a focus of atmospheric science for several decades due to their effect on primary ice formation in clouds. While pure cloud droplets freeze homogeneously at $\sim -37\,^\circ\mathrm{C}$ (Pruppacher and Klett, 1997), the freezing onset is shifted towards higher temperatures in the presence of INPs. With that, INPs influence cloud properties such as the radiative effect and lifetime, as well as precipitation formation (Creamean et al., 2013; Michaud et al., 2014; Vergara-Temprado et al., 2018; Lin et al., 2022). An accurate representation of INP concentrations, i.e., the number of INPs active at a certain temperature per volume of air, could help decrease the currently large uncertainty of the effect of clouds and aerosol–cloud interactions on Earth's radiative budget in climate models (Forster et al., 2021). Using aerosol particle properties to predict INP concentrations is subject to ongoing research (Phillips et al., 2013; DeMott et al., 2015; Fitzner et al., 2020), albeit a difficult task, since it is still not completely understood what makes certain parti-

cles more efficient at nucleating ice than others. In any case, a sound database for the verification of parametrizations of INP concentrations is necessary which requires atmospheric measurements of INP concentrations. Remote locations, especially the Arctic, Antarctica, the Southern Ocean, and the free troposphere, have not yet been sufficiently studied to provide conclusive INP parametrizations (Murray et al., 2021).

Nonetheless, the amount of INP concentration data generated has increased tremendously in recent years first and foremost due to the development of a large number of different instruments for offline immersion-freezing characterization (DeMott et al., 2011, 2018). In contrast to complex online instrumentation, e.g., continuous-flow diffusion chambers (CFDCs; Rogers, 1988; Stetzer et al., 2008; Garimella et al., 2016), these are relatively easy to set up and use sampling volumes that are several orders of magnitude larger, enabling the investigation of rare, high-temperature ($\geq -15\,°C$) INPs which are not captured by online instruments. Some offline techniques operate with microliter-sized droplets on glass substrates (Budke and Koop, 2015; Whale et al., 2015; Chen et al., 2018) or in separate wells (Conen et al., 2012; Hill et al., 2014) and usually cannot produce meaningful data below $\sim -30\,°C$ due to freezing induced by impurities (measurement background). Others use nanoliter- or picoliter-sized droplets which shift the freezing onset temperature of pure water droplets towards the homogeneous freezing limit (Pummer et al., 2012; Wright and Petters, 2013; Peckhaus et al., 2016; Stan et al., 2009; Riechers et al., 2013; Reicher et al., 2018). All of these techniques can be operated with aqueous suspensions such as collected sea water (Wilson et al., 2015; Irish et al., 2017), river water (Knackstedt et al., 2018; Moffett, 2016), cloud water (Joly et al., 2014), precipitation samples (Petters and Wright, 2015), impinger samples (Šantl-Temkiv et al., 2017), impactor samples (Mason et al., 2016; Reicher et al., 2019), or washing water of filter samples (McCluskey et al., 2018; Adams et al., 2020; Hartmann et al., 2021; Jakobsson et al., 2022). Some offline instruments also use punched-out pieces of filter material with collected aerosol particles immersed in water (Conen et al., 2012; Welti et al., 2018). By using a combination of offline instruments featuring different droplet sizes, it is possible to span a broad range of INP concentrations in a temperature regime of which only the lowermost bound can be covered with the online techniques.

Automatic aerosol particle sampling equipment is commercially available, low maintenance, and hence operated frequently in ground- or ship-based measurement campaigns as well as in long-term measurements to obtain INP concentrations (Schrod et al., 2020; Schneider et al., 2021; Testa et al., 2021; Sze et al., 2023). While ground-based aerosol particle sampling is an important step towards revealing the nature and sources of INPs, open questions exist concerning the mechanisms making INPs airborne, the vertical transport of INPs, their concentrations at cloud level, and

their influence on cloud formation and properties (Coluzza et al., 2017). Furthermore, the influence of cloud processing on INP concentrations and the relative abundance of INPs in cloud particle residuals have rarely been investigated (Stopelli et al., 2015; Levin et al., 2019). In situ measurements of free tropospheric INPs are generally sparse, as they can only be performed on mountain sites (DeMott et al., 2003a; Lacher et al., 2018; Conen et al., 2022) or with the help of airborne platforms. Creamean et al. (2018) and Porter et al. (2020) describe aerosol particle sampling for ice nucleation analysis with the help of tethered balloons, which, in contrast to a stationary measurement site, offer flexibility regarding the sampling altitude but have restricted payloads of a few kilograms at most. The same holds for aerosol particle samplers deployed on small unoccupied aerial vehicles (Schrod et al., 2017; Jimenez-Sanchez et al., 2018; Bieber et al., 2020). Alternatives to the described approaches are INP measurements on research aircraft which can reach the upper troposphere and are typically equipped with a large instrument suite for answering specific research questions. Consequently, there are simultaneous measurements of, for example, meteorological parameters, aerosol particle properties, and trace gases, which can contribute to the interpretation of the INP results. Both online methods, i.e., CFDCs (Rogers et al., 1998, 2001; DeMott et al., 2003b; Levin et al., 2019; Barry et al., 2021b), and offline methods, i.e., filter sampling systems (Bigg, 1967; Flyger et al., 1973; Borys, 1989; DeMott et al., 2016; Price et al., 2018; Levin et al., 2019; Sanchez-Marroquin et al., 2020, 2021; Varble et al., 2021; Barry et al., 2021b), have been used on board aircraft. Online methods provide the benefits of better time resolution compared to filter samples and the possibility to investigate different nucleation modes depending on the thermodynamic conditions in the measurement chamber. Unfortunately, changing conditions takes some time, with the duration depending on the planned temperature and/or humidity step, which restricts flexibility (Rogers et al., 2001). Furthermore, most online instruments work with low flow rates of $\sim 1\,L\,min^{-1}$ (Rogers, 1988; Stetzer et al., 2008; Garimella et al., 2016), meaning that high-time-resolution data are restricted to below $\sim -25\,°C$ where INP concentrations are above the detection limit. Additional disadvantages are the large dimensions of online instrumentation, which can conflict with common space and weight restrictions on board aircraft. In contrast, aerosol particle filter samples can be collected with comparably small, light-weight equipment. As offline INP measurements are suitable for generating INP concentration data between 0 and $\sim -30\,°C$ and even down to $-37\,°C$ when nanoliter-sized droplets are used, they are a valuable addition to online INP measurements on board aircraft.

All of the abovementioned studies describing aerosol particle filter sampling on board aircraft for offline INP analysis use commercially available filter holders or modifications of those, which are exposed to ambient air from the outside of

the aircraft via an inlet system and sampling line. Changing filters during flight involves manual valve operation, removal of the sampled filters and their holders, and insertion of previously prepared filter holders with clean filters (Bigg, 1967; Flyger et al., 1973; Borys, 1989; DeMott et al., 2016; Price et al., 2018; Levin et al., 2019; Sanchez-Marroquin et al., 2020, 2021; Varble et al., 2021; Barry et al., 2021b). This approach comes with several drawbacks. Firstly, there is no possibility of automation and an on-board operator has to perform the filter changes. Secondly, contamination could be introduced to the samples during the handling of the filter holders during flight. Last but not least, removing equipment from the aircraft during flight is not always allowed from an aviation certification point of view. The collection of field blanks on board aircraft, which is essential for estimating background levels in the immersion-freezing experiments, has been described by Borys (1989), Levin et al. (2019), Barry et al. (2021b), and Sanchez-Marroquin et al. (2021). The blanks were handled in the same way as the filter samples, i.e., prepared in the laboratory, placed inside a clean filter holder, and connected to the sampling line during flight but without air exposure. While no significant contamination was reported in the abovementioned studies, blanks were not taken during every flight, and contamination might have been missed, depending on the frequency of occurrence. Concerning volumetric flow rates through the filters, values of $\sim 10\,\mathrm{L\,min^{-1}}$ (Borys, 1989; DeMott et al., 2016; Sanchez-Marroquin et al., 2019) or less (Levin et al., 2019; Barry et al., 2021b) were reported. One exception is the study by Flyger et al. (1973), who sampled at a rate of more than $50\,\mathrm{L\,min^{-1}}$. Generally, a high flow rate is desirable, as INP numbers above the measurement background can be collected in a shorter period of time. Consequently, more filters can be sampled per flight, and there is an increase in temporal and spatial resolutions. In previous studies, the flow through the filters was generated by pumps downstream of the filter holders supported by the ram pressure of the moving aircraft (Flyger et al., 1973; Price et al., 2018; Sanchez-Marroquin et al., 2020, 2021). However, none of the setups included active control of the pump speed, which would be another step towards automation and would make the systems more versatile for isokinetic sampling on a range of different aircraft with differing inlet and sampling line designs.

In this paper, we describe the design and performance of the novel High-volume flow aERosol particle filter sAmpler (HERA) which was specially developed for aircraft application and offline INP analysis. In contrast to the abovementioned sampling methods, HERA is highly automated. Up to six filters can be loaded into the device prior to takeoff and selected during flight via an electric motor controlled by software. This design eliminates manual filter handling and lowers the potential for contamination. One of the six slots can be reserved for a field blank for background correction. HERA also features a powerful actively controlled pump unit downstream of the filters which can generate flow rates exceeding

$100\,\mathrm{L\,min^{-1}}$, depending on the selected filter medium and the pressure conditions. A prototype of HERA was successfully deployed during PAMARCMiP (Polar Airborne Measurements and Arctic Regional Climate Model simulation Project) in late winter 2018 (Hartmann et al., 2020). Afterwards, the system was revised and characterized in the laboratory and field. While the HERA filter samples can be used for a number of different types of aerosol particle analyses, e.g., scanning electron microscopy for particle morphology analysis (Sanchez-Marroquin et al., 2021; Seifried et al., 2021) or ion chromatography for bulk chemical composition analysis (Kwiezinski et al., 2021), this study focuses on the application for immersion INP measurements. In the following, we present the technical description of HERA, characterization experiments with standard and atmospheric INPs, and first results from sampling of HERA on board aircraft during the HALO (High Altitude and LOng range research aircraft) mission CIRRUS-HL (cirrus in high latitudes). Materials and experimental methods relating to the sampling are described separately in the upcoming three sections, followed by the results and their discussion. Details concerning the offline immersion INP analysis are given in Appendix A.

2 Instrument description

2.1 Design

HERA was conceptualized and built by Enviscope GmbH (Frankfurt, Germany) in close collaboration with the Leibniz Institute for Tropospheric Research (TROPOS; Leipzig, Germany). Figure 1a shows a schematic of the installation on board the aircraft using the example of the HALO CIRRUS-HL mission. HERA consists of a sampling unit and pump unit. The sampling unit is connected to an inlet, which is the HALO Submicrometer Aerosol Inlet (HASI) in the case of HALO, through which ambient aerosol particles are collected. If available, as during CIRRUS-HL, HERA can also sample from a second inlet, e.g., a counterflow virtual impactor (CVI; Ogren et al., 1985; Mertes et al., 2007) for in-cloud sampling of residual particles. In this case, electrical valves are installed and controlled via software to open or close the connection to the respective inlets.

The sampling unit measures $49\,\mathrm{cm} \times 52\,\mathrm{cm} \times 27\,\mathrm{cm}$ (width $\times$ depth $\times$ height), fits into a standard 19 in. rack unit, and weighs 22 kg. It houses an insert containing six metal filter holders which, together with a bypass tube, are arranged concentrically around a shaft connecting two seven-way valves (see photo Fig. 1b and cross section in Fig. 1c). The valves are turned in unison via a chain drive connected to a servo motor, and the valve position is set remotely via software. As a result, air flows through two 90° bends onto one distinct filter (see Fig. 1c). The valve construction involved careful consideration of the design and materials to avoid leaks among the filter positions and from HERA to the
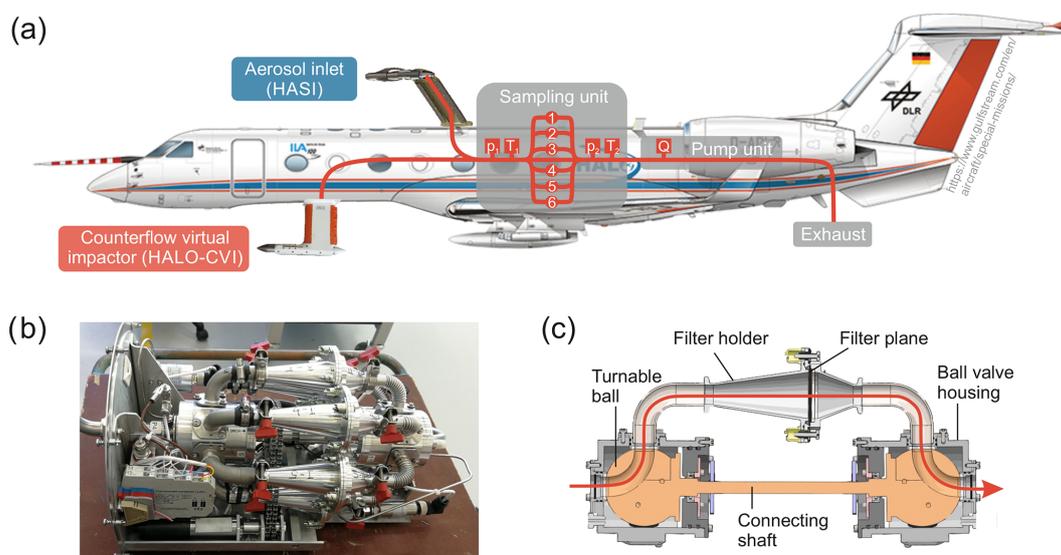
Figure 1. (a) Installation of HERA on the HALO research aircraft. The sampling unit can be connected to either the aerosol particle inlet (HASI) or the counterflow virtual impactor (HALO-CVI) for sampling outside or inside clouds. Switching between inlets is performed remotely with electrical valves. **(b)** Photo of the filter holder insert of the HERA sampling unit. **(c)** Cross section of one of the six filter holders connected to the seven-way valves. The red line indicates the center streamline of the air flow through the system.

ambient environment. Two sets of temperature and pressure sensors prior and post filter record the inline thermodynamic conditions. Furthermore, the sampling unit contains the data acquisition and control computer. The pump unit measures $49\,\text{cm} \times 25\,\text{cm} \times 18\,\text{cm}$, weighs 13 kg, and is equipped with three oil-free vacuum scroll pumps (SVF-E0-50PF, Scroll Labs, USA). Each of them is able to generate a flow rate of $50\,\text{L}\,\text{min}^{-1}$ for undisturbed standard conditions, i.e., a maximum flow rate of $150\,\text{L}\,\text{min}^{-1}$ can be achieved. At full pump speed, the power rating of HERA is $\sim 400\,\text{W}$. Generally, HERA can be operated with different filter media, such as quartz fiber filters or polycarbonate (PC) membrane filters, with a diameter of 47 mm. In this work, we only present experiments with PC filters (Nuclepore™ track-etched membranes, Whatman, UK), which are frequently used for INP sampling due to their smooth surface from which particles can be washed off with high efficiency (e.g., DeMott et al., 2016; Tarn et al., 2018). Furthermore, PC filters are chemically inert, making them suitable for pre-treatments (Hill et al., 2017). At a constant inlet flow rate and unchanging number of pores, a smaller pore size filter always leads to a larger pressure drop and hence an increase in pump speed in comparison to a larger pore size filter (Liu and Lee, 1976; Zíková et al., 2015). This relation, together with the inlet-specific flow rate requirements, must be kept in mind when selecting the filter medium. See Sect. 3.1 for a more detailed discussion of the effect of PC filter pore size on INP sampling. The pump unit also contains a mass flow meter (4043, TSI Inc., USA) upstream of the pumps whose data, together with the inline temperature and pressure measurements in the sampling unit, are used to calculate the volumetric flow

rate at the HERA inlet. The maximum error in flow rate, as estimated by error propagation, utilizing the manufacturer-specific accuracies of the temperature and pressure sensors and the flow meter, is $\sim 3\,\%$. The pumps are actively controlled to keep the inlet volumetric flow rate constant, independent of pressure and temperature changes. The flow rate is controlled remotely via software to maintain a setup-specific value (e.g., $40\,\text{L}\,\text{min}^{-1}$ at the HASI during CIRRUS-HL) and set to zero during turning of the valve to select a new filter position.

2.2 Theoretical sampling characteristics

The general goal when sampling aerosol particles is the minimization of particle losses and enrichment so that the collected particles are comparable to the ambient aerosol in terms of their physicochemical properties. The overall sampling efficiency is influenced by the aspiration efficiency of particles in the inlet and the transmission efficiency in the tubing, both of which are strongly dependent on the particle size and mass (Brockmann, 2011). Generally, small particles ($\lesssim 100\,\text{nm}$) are prone to diffusional losses, whereas larger particles are lost due to inertial and gravitational forces. While there are several factors influencing the potential of an aerosol particle to act as an INP, size seems to be an important one, as the concentration of large particles has been shown to correlate with the INP concentration (Pruppacher and Klett, 1997; DeMott et al., 2010). INP sampling should hence be set up so that losses of large particles are minimized. Simultaneously, care must be taken to sample isokinetically, i.e., to align the inlet in the main wind direction and

match the inlet face velocity to the velocity of the surrounding air. The latter is especially a challenge on board aircraft, as the velocity of the aircraft relative to the air mass, i.e., the true air speed (TAS), usually varies with flight altitude. If the sample flow velocity is lower than the TAS, sampling is sub-isokinetic and particles with a sufficiently large inertia are oversampled. In contrast, there is super-isokinetic sampling (sample flow velocity higher than TAS), where particles with a sufficiently high inertia are undersampled (Brockmann, 2011).

For the design of HERA, the layout and inner diameter of the tubing leading up to the filter surface needed to be optimized with respect to the target flow rate and pressure regime to minimize gravitational settling and impaction of supermicron particles due to inertia. Figure 2 shows the transmission efficiency of particles in HERA in a size range from 0 to 20 μm for different volumetric flow rates ranging from 5 to 100 L min^{-1} at two pressure levels (1013 and 200 mbar). These calculations only include the transmission efficiency from the HERA inlet to the filter surface. Calculations were performed with the Particle Loss Calculator (von der Weiden et al., 2009), assuming spherical particles with a density of 2 g cm^{-1} and a temperature of 20 °C. The inner tube diameter leading up to the filter holders is 16.57 mm. It can be seen that there is a strong dependency of the transmission efficiency on the flow rate, with lower flow rates causing fewer losses of supermicron particles due to reduced impaction in the bends. Exceptions are very low flow rates of ≤ 5 L min^{-1}, where the lower flow velocity causes stronger gravitational settling in comparison to sampling at 10 L min^{-1}. At a flow rate of 10 L min^{-1}, 50 % of particles with a diameter of 11.4 μm (D_{50}) are transmitted, whereas D_{50} is shifted to 7.0 μm at 40 L min^{-1}. For flow rates higher than ~ 60 L min^{-1}, the flow within HERA becomes turbulent for near-surface pressure conditions, leading to a decrease in transmission efficiency for the majority of the particle size distribution. At low pressure, laminar flow conditions can be maintained for flow rates between 60 and 100 L min^{-1} with D_{50} values of 5.7 and 4.4 μm, respectively. Diffusional losses are negligible for particles larger than 100 nm (transmission efficiency ≥ 99.5 % for the shown range of flow rates and pressures).

To summarize, the HERA geometry theoretically allows for efficient supermicron particle sampling over a wide range of flow rates and pressure levels. Note that D_{50} is expected to shift to smaller particle diameters when including the aspiration efficiency of the aircraft inlet and particle transport in the sampling line leading up to the instrument (see Sect. 4 for CIRRUS-HL particle losses). Hence, the positioning of HERA on board aircraft with respect to the inlet and the geometry of the sampling lines should be carefully planned in such a way as to minimize particle losses. Eventually, particle loss calculations can be used, together with simultaneous measurements of the aerosol particle size distribution, to correct the size distribution of particles sampled on the filters in HERA.
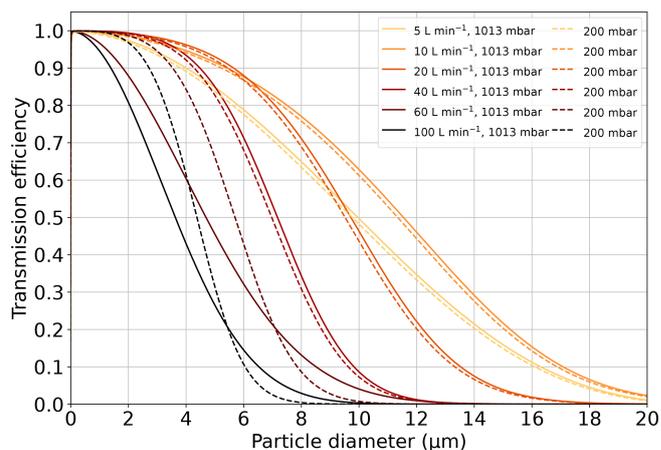
Figure 2. Transmission efficiency of spherical particles with a density of 2 g cm^{-1} at 20 °C from the HERA inlet to the filter surface at two different pressure levels (solid lines: 1013 mbar, dashed lines: 200 mbar) as a function of the volumetric flow rate. Lighter colors mark lower flow rates; darker colors mark higher flow rates. Refer to Sect. 4 for sampling efficiencies during CIRRUS-HL.

2.3 Operation

After a research flight, the HERA sampling unit is disconnected from the inlet sampling line and the exhaust line to the pump unit. Only the filter insert is removed from the aircraft and sealed for transport to the laboratory. Filters are removed from their holders under a laminar flow hood, packaged in petri dishes (Analyslide®, PALL cooperation, USA), and kept frozen at −20 °C until used for offline immersion INP measurements with the Leipzig Ice Nucleation Array (LINA) and the Ice Nucleation Droplet Array (INDA; see Appendix A for details). At least one of the six filters is reserved as a blank, i.e., a filter which is handled in the same way as the others but is not sampled. This procedure ensures that contaminations are registered and provides a flight-specific background level against which the INP spectra of the corresponding filter samples can be compared. The filter holders are cleaned after each flight in an ultrasonic bath in ultrapure water with a low percentage of ethanol and dried with pressurized, filtered air. Common guidelines for INP-specific filter handling, storage, and measurements were taken into consideration (Polen et al., 2018; Beall et al., 2020; Barry et al., 2021a). Filter treatments described in the literature (Barry et al., 2021a) did not lower the measurement background of LINA and INDA, which is why filters were used as provided by the manufacturer in all here-presented experiments.

Any kind of aircraft INP filter sampling involves careful planning to achieve truly meaningful sampling intervals. In general, the flight pattern should be accounting for sampling periods under somewhat constant atmospheric conditions, e.g., staircase ascents or descents with several minutes of flight time in a constant altitude. The measured INP concen-

tration can be later affiliated with these constant conditions, which facilitates the interpretation of results as compared to averaging over a range of different conditions (Coluzza et al., 2017). Height-resolved sampling below, inside, and above a cloud layer could give insight about the effect of the available INPs on the formation of the cloud. Comparing filters sampled in different air masses or above contrasting surface features might hint towards the source of the INPs. In practice, the sampling strategy often must be adapted during flight due to unforeseen changes in weather conditions and/or flight track. Consequently, fast decisions by the on-board operators are needed which can be easily realized with HERA due to the quick (< 30 s) and remote-controlled switching between filters. The capacity of six filters per flight was based on typical flight durations and expected INP concentrations in the free troposphere, and so far it has been found to be appropriate in practice. If more filters are needed and the aircraft certification regulations allow for it, the filter holder insert could be removed during flight and filter holders could be exchanged.

Differences in the total sampling volume translate to differences in the range of measurable INP concentrations (see Fig. 3). Each box shows the measurable INP concentration range for a specific sampling time at a flow rate of $40 \, \text{L min}^{-1}$ for either LINA (bluish colors) or INDA (reddish colors), derived from the instrument-specific minimum and maximum measurable frozen fractions, droplet volumes, and filter washing water volumes. The flow rate of $40 \, \text{L min}^{-1}$ was chosen according to the flow rate at the HASI during the CIRRUS-HL campaign (see Sect. 4). LINA and INDA together span an INP concentration range of ~ 4 orders of magnitude, which can be seen when comparing the upper and lower limits of boxes with the same line style. A shift from the low- to the high-temperature regime (and with that from the high to the low-INP-concentration regime) occurs with an increase in sampling time, i.e., sampling volume. Nonetheless, apparently already a very short sampling time of 1 min (solid line) is sufficient to capture high-temperature INPs with INDA if present at concentrations of more than $0.03 \, \text{L}^{-1}$. However, a very small number of INPs per filter would be related to a large statistical uncertainty, while longer sampling times increase the number of INPs per filter and produce data with a higher statistical significance. Furthermore, one must take the measurement background into account. For INDA, this background is negligible at $-10\,°\text{C}$ but increases to ~ 5 INPs per rinsed filter at $-20\,°\text{C}$. As a consequence, a sampling time of at least 10 min (dashed line) is necessary to collect a sufficient number of INPs on the filter for INDA measurements above the background at $-20\,°\text{C}$. The high INP concentration regime at temperatures below $-20\,°\text{C}$ can be investigated with LINA due to the smaller droplet size and/or dilution of the filter extracts with ultrapure water as long as the background of the instruments allow for it.
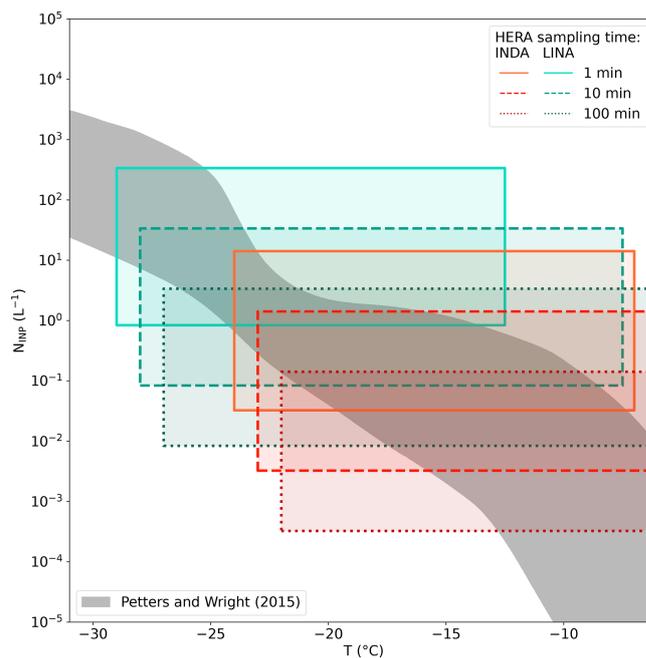
Figure 3. Measurable INP concentrations (N_{INP}) of INDA (reddish colors) and LINA (bluish colors) when operated with HERA filter extracts. Different sampling times between 1 min (solid lines) and 100 min (dotted lines) with a flow rate of $40 \, \text{L min}^{-1}$ were assumed. Washing water volumes of 6.2 mL (INDA) and 3.0 mL (LINA) and droplet volumes of $50 \, \mu\text{L}$ (INDA) and $1 \, \mu\text{L}$ (LINA) were considered. Note that due to background effects, INDA and LINA are limited towards low temperatures, which is approximated by the left margins of the drawn boxes. The limits towards high temperatures (right margins) are approximated from the intersections with the upper limit of atmospheric INP concentrations derived from mid-latitude precipitation samples (grey area in the background; Petters and Wright, 2015).

3 Characterization experiments

3.1 Effect of filter pore size on INP sampling

Collection efficiencies of PC filters have frequently been measured (Spurny and Lodge, 1972; Burton et al., 2007; Zíková et al., 2015; Soo et al., 2016). For example, 400 nm pore size filters have proven to collect more than 98 % of aerosol particles with diameters between 10.4 and 412 nm across a range of flow rates varying between 1.7 and $11.2 \, \text{L min}^{-1}$ (Soo et al., 2016). An even higher sampling efficiency is to be expected for filters with a pore size of 200 nm, which are often used for ground-based INP sampling at flow rates below $30 \, \text{L min}^{-1}$ (DeMott et al., 2016; Knackstedt et al., 2018; Tobo et al., 2019; Tatzelt et al., 2022). However, pre-tests with this filter type have resulted in structural damage of the filter material at $40 \, \text{L min}^{-1}$ and low pressure (200 mbar), which is why the use of larger pore size filters was considered for HERA. At near-standard pressure, up to $120 \, \text{L min}^{-1}$ can be generated through a 800 nm pore

size filter with the HERA pump unit. At 200 mbar, the maximum volumetric flow rate through 800 nm pore size filters decreases to $\sim 60\,\mathrm{L\,min^{-1}}$.

To investigate the efficiency of 800 nm pore size filters in the context of INP sampling, we used two of the TROPOS-built High-volume And Light-weight Filter samplers for BAlloon-borne appliCation (HALFBAC) and equipped one with a 200 nm pore size filter and the other one with a 800 nm pore size filter. HALFBAC consists of a filter holder (47 mm, 1/2 in. inlet; PFA, Savillex, MN, USA); a vacuum scroll pump (same as in HERA pump unit); temperature, pressure, and relative humidity sensors; radio antenna; GPS module; data logger; and a set of lithium polymer batteries, all contained in a weatherproof housing and weighing below 4.5 kg. The flow rate in HALFBAC is not actively controlled but adjusted via the pump speed prior to sampling while measuring with an external flow meter. Flow rates during sampling are recorded indirectly in the form of differential pressure within a capillary downstream of the filter holder.

Firstly, filters were sampled with polydisperse Arizona Test Dust particles (ATD, nominal fraction 0–3 µm; Powder Technology Inc., USA) generated from a suspension with an atomizer (similar to 3076, TSI Inc., USA). The suspension was produced by mixing 2.6 g ATD in 50 mL ultrapure water (Milli-Q, $18.2\,\mathrm{M\Omega\,cm^{-1}}$) and shaking for 15 min. After a settling time of 5 min, the top half of the initial suspension was decanted for further use. The two HALFBAC instruments were connected to the aerosol sampling line to deposit particles onto both filter types in parallel at a volumetric flow rate at the inlet of $15\,\mathrm{L\,min^{-1}}$ generated by the built-in scroll pumps. Secondly, the two HALFBAC instruments were used to sample urban-influenced, continental air on the roof of the Cloud Laboratory at TROPOS in Leipzig, Germany, on 22 February 2021. Note that for the ambient sampling, both HALFBAC instruments sampled through their individual inlets which were pointed into the main wind direction. Conductive silicone tubing was added to the inlets to reduce the probability of particle losses due to electrostatic attraction. The filters were sampled simultaneously for 30 min at a volumetric flow rate of $15\,\mathrm{L\,min^{-1}}$. This comparably low flow rate was chosen to allow for prolonged sampling through the 200 nm pore size filters with the battery-powered HALFBAC. The immersion INP analysis was performed with INDA and LINA according to the standard method described in Appendix A.

The number of INPs per filter with respect to temperature can be seen in Fig. 4. Note that here and in the following error bars in y direction only represent the uncertainty of the immersion-freezing measurements as described in Appendix A, which is significantly larger than the maximum error in sampling volume (see Sect. 2.1). Error bars are only shown for every fifth data point for better clarity. In the case of the polydisperse ATD particles (left panel), the measured number of INPs per filter is independent of the filter pore size. The slight differences in the number of INPs observed

at a temperature above $-18\,^{\circ}\mathrm{C}$ are within measurement uncertainty. Also in the case of the ambient aerosol particles (right panel), both filter types apparently collected comparable numbers of INPs. However, the agreement is much better for the INDA measurements above $-18\,^{\circ}\mathrm{C}$ than for the LINA measurements at lower temperatures. The steeper slope of the INP spectrum of the 800 nm pore size filter in comparison to the 200 nm pore size filter below $-18\,^{\circ}\mathrm{C}$ is unresolved but could stem from differences in aspiration efficiency due to the lack of a common inlet. Variations in wind speed and direction influence the overall sampling efficiency (see Sect. 3.3) and could have affected both HALFBAC instruments to different degrees during the rooftop sampling. However, it seems unlikely that only low-temperature INPs would be affected by this. The described deviation is definitely not related to a lower sampling efficiency of the 800 nm pore size filters, since the number of collected INPs on this filter type is higher in comparison to the 200 nm pore size filter below $-21\,^{\circ}\mathrm{C}$. The statement that 800 nm pore size filters are just as well suited to collect atmospheric INPs as 200 nm pore size filters is supported by the fact that the INP numbers agree within measurement uncertainty for polydisperse ATD particles and ambient particles above $-21\,^{\circ}\mathrm{C}$. Our results coincide with measurements by Lacher et al. (2023), who also present comparable results of INP measurements with 200 and 800 nm pore size filters from identical sampling periods. Note that an increase in flow rate would even lead to an improved filter efficiency over all particle sizes (Zíková et al., 2015; Soo et al., 2016). Based on these measurements, all of the following results were retrieved using PC filters with 800 nm pore size for particle sampling.

3.2 Collection efficiency of size-selected standard INPs

In order to verify the theoretical particle transmission efficiencies for different particle sizes and flow rates, laboratory experiments with test substances were performed. This was done via immersion INP filter analysis, which is the typical HERA use case. Briefly, aerosol particles were generated from a suspension with an atomizer, dried, size-selected by sending them through a neutralizer and differential mobility analyzer (DMA, Vienna type, medium), mixed with particle-free pressurized air to increase the flow rate, and sampled onto filters with HERA. The number concentration of the particles in the sampled air was registered with a condensation particle counter (3010, TSI Inc., USA). Together with the electrical mobility diameter set at the DMA and the sampling flow rate set at the HERA pump unit, the particle surface area and mass per filter was determined by assuming spherical particles. Due to the particle generation setup, the sampling experiments were restricted to particles with mobility diameters ≤ 800 nm, where particle losses should be minimal according to the theoretical calculations (see Fig. 2, minimum transmission efficiency of 96.4 % for 800 nm particles sampled at a flow rate of $100\,\mathrm{L\,min^{-1}}$ and near-standard
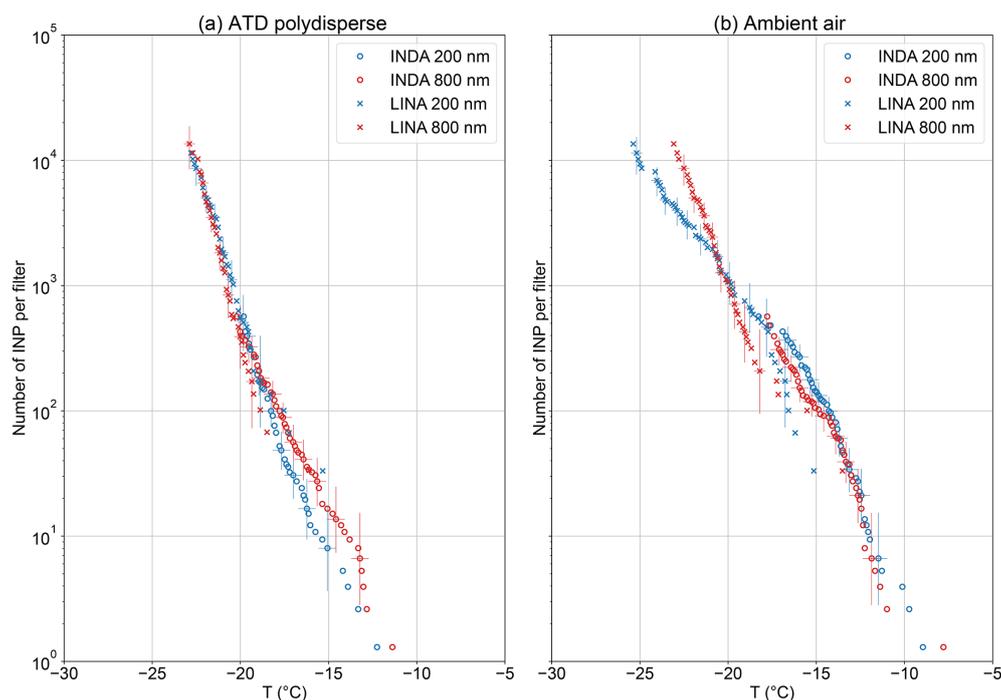
Figure 4. Number of INPs detected on filters sampled with polydisperse ATD **(a)** and urban ambient air **(b)**. Filters with 200 (blue) and 800 nm pore size (red) were sampled simultaneously in two HALFBAC instruments and analyzed with INDA (circles) and LINA (crosses). Note that a common inlet was used for ATD particle sampling whereas each filter was sampled through an individual inlet for ambient aerosol particle sampling. The volumetric flow rate at the HALFBAC inlet was $15\,\text{L}\,\text{min}^{-1}$ in all cases.

pressure). Regarding supermicron particles, a decrease in transmission efficiency is expected according to the calculations, but experimental results cannot yet be provided.

Two substances, SNOMAX® (SMI Snow Makers AG, Switzerland) and ATD, were used for particle generation to investigate the sampling efficiency of INPs of both biological and mineral origin at near-standard pressure conditions. SNOMAX® is a commercially available freezing catalyst containing nonviable cells and fragments of *Pseudomonas syringae* bacteria. The SNOMAX® suspension was generated by dissolving 0.1 g in 50 mL ultrapure water. The ATD suspension was generated in the same way as described in Sect. 3.1. In total, three different particle sizes (300, 500, 800 nm) were sampled at three different flow rates (10, 40, $100\,\text{L}\,\text{min}^{-1}$) for both substances. The positions of the filters in the HERA sampling unit were rotated between trials so that each of the six positions was used equally in the course of the sampling experiments. For the immersion-freezing experiments, the SNOMAX® filters were rinsed with 6 mL ultrapure water, then five 10-fold dilutions of the original extract were produced and investigated with INDA. The ATD filters were measured with INDA and LINA according to the standard method (see Appendix A).

Figure 5 shows the results of the filter sampling and immersion-freezing measurements with SNOMAX® particles of different monodisperse diameters sampled at different flow rates with HERA. To calculate the ice-nucleation-

active site density per unit mass n_{m}, a SNOMAX® density of $1.35\,\text{g}\,\text{cm}^{-3}$ was used (Wex et al., 2015). Each n_{m} spectrum is made up of six individual INDA measurements of the subsequent dilution steps. Of these combined n_{m} spectra, each is shown twice. Firstly, they are shown in the top row to view potential effects of the flow rate on the sampling of differently sized monodisperse particles with diameter D_{p}. Secondly, they are shown in the bottom row to compare filters sampled with differently sized monodisperse particles at a constant flow rate Q. Overall, we observe good agreement of the n_{m} spectra of experiments with different particle diameters and flow rates. For example, the 300 nm particles sampled at a flow rate of $10\,\text{L}\,\text{min}^{-1}$ yielded similar n_{m} values as the 300 nm particles sampled at a flow rate of $100\,\text{L}\,\text{min}^{-1}$. The 300 nm particles sampled at a flow rate of $100\,\text{L}\,\text{min}^{-1}$, in turn, yielded similar n_{m} values as the 800 nm particles sampled at a flow rate of $100\,\text{L}\,\text{min}^{-1}$. Significant particle losses and/or leaks would lead to a particle-size- or flow-rate-dependent decrease in n_{m}, which we did not observe. This finding is in line with the results of the transmission efficiency calculations (see Sect. 2.2).

On another note, Polen et al. (2016) describe a decrease in ice nucleation efficiency of SNOMAX® over time, even if the sample was continuously stored at $-20\,°\text{C}$. This is significant, since our SNOMAX® batch was more than 3 years old when the sampling experiments took place. We hence chose to compare the n_{m} values from the HERA sampling
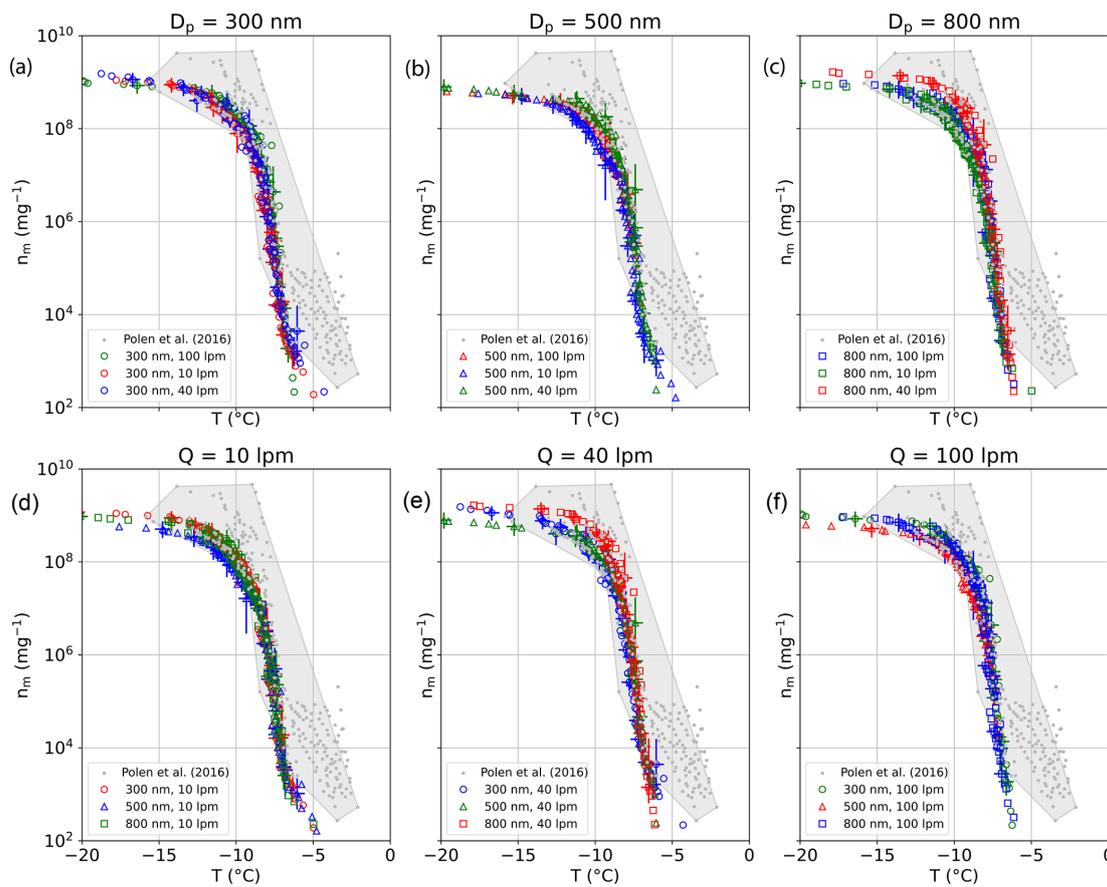
Figure 5. Ice-nucleation-active site density per unit mass n_m with respect to temperature for monodisperse SNOMAX® particles of different diameters sampled at different flow rates with HERA. Each panel in the top row (**a–c**) shows results for one particle diameter (D_p, circles: 300 nm, triangles: 500 nm, squares: 800 nm) at three different flow rates (Q, red: 10 L min^{-1}, blue: 40 L min^{-1}, green: 100 L min^{-1}). Each panel in the bottom row (**d–f**) shows results for one flow rate and three different particle diameters (colors and marker shapes as in top row). Data framed in grey in the background were extracted from Polen et al. (2016) using a plot digitizer (Rohatgi, 2022).

with measurements from Polen et al. (2016) of a batch that was roughly 1 year old instead of comparing to a fresh batch. Data by Polen et al. (2016) were generated by producing 0.1 µL droplets from SNOMAX® suspensions with different concentrations and cooling them down in an oil matrix. The here-presented n_m data lie within the envelope of measurements with "old" SNOMAX® by Polen et al. (2016, grey background in Fig. 5). This means that a similar number of active sites per mass is found in droplets from SNOMAX® suspensions and in washing water of filters sampled with SNOMAX® particles, i.e., INPs in submicron SNOMAX® particles are sampled efficiently with HERA. Interestingly, we do not observe the freezing mode above −5 °C, reported by Polen et al. (2016) and in earlier studies (Maki et al., 1974; Yankovsky et al., 1981; Turner et al., 1990; Budke and Koop, 2015), which can have several causes. This mode is commonly associated with the occurrence of large aggregates of ice-nucleation-active proteins which are found in the outer membranes of the *P. syringae* bacteria (Lindow, 1995; Schmid et al., 1997). Bacterial cells have been shown

to break into fragments when spraying a SNOMAX® suspension with an atomizer (Wex et al., 2015), reducing the probability of large protein aggregates being deposited on the filters. Another reason for the missing high-temperature mode could be the prolonged storage of the SNOMAX® batch, leading to some kind of deactivation of the large protein complexes.

Monodisperse ATD particles were sampled equivalently to the SNOMAX® experiments but were investigated with both INDA and LINA according to the standard method (see Appendix A), foregoing the dilution series. It is interesting to note that, following the sampling experiments with SNOMAX®, the particle generation setup and HERA had to be thoroughly cleaned twice before no more SNOMAX® signatures were observed in the immersion INP analysis. Figure 6 shows the results of the immersion-freezing experiments with 300, 500, and 800 nm particles sampled at 10, 40, and 100 L min^{-1}. In contrast to the SNOMAX® results, n_s was calculated from the total particle surface area of ATD per filter, which is a better measure of ice nucleation ef-
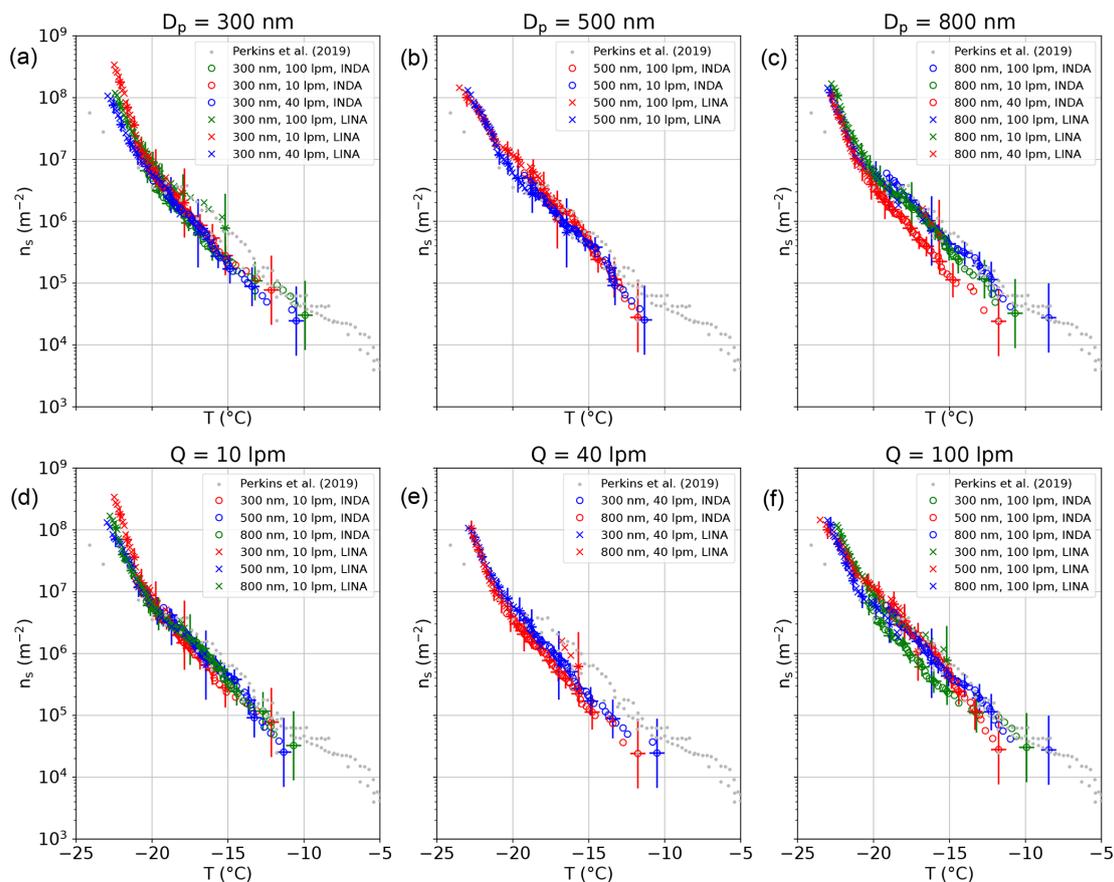
Figure 6. Ice-nucleation-active surface site density n_s with respect to temperature for monodisperse ATD particles of different diameters sampled at different flow rates with HERA. Circles show data retrieved from INDA measurements; crosses show data from LINA measurements. Each panel in the top row **(a–c)** shows results for one particle diameter at three different flow rates. Each panel in the bottom row **(d–f)** shows results for one flow rate and three different particle diameters (colors as in top row). The grey data points in the background were extracted from Perkins et al. (2019) using a plot digitizer (Rohatgi, 2022).

ficiency than n_m in the case of largely insoluble materials such as mineral dust (Connolly et al., 2009). Again, each n_s spectrum is shown twice for better visualization of potential effects of particle diameter and flow rate on n_s. Equally to the SNOMAX® results, the ATD n_s spectra are similar to one another in their shape and magnitude. It appears that the spread between the different experiments is highest for the largest particle diameter (800 nm) and the highest flow rate (100 L min^{-1}). However, even in these cases, most data points are found within the range of measurement uncertainty, and no clear trend in the magnitude of n_s with particle size or flow rate is observed. Furthermore, our results agree well with data by Perkins et al. (2019), who measured the immersion-freezing behavior of 50 µL aliquots of ATD suspensions with different concentrations with a PCR-tray-based system. Note that for the comparison ATD n_m values from Perkins et al. (2019) were converted to n_s using the specific surface area of fine ATD of 4 m^2 g^{-1} (Cwiertny et al., 2008). If INPs would be lost during sampling with HERA, this would result in a lower number of active sites per surface

area in comparison to the results by Perkins et al. (2019). In conclusion, HERA is suited for representative sampling of submicron ATD particles for subsequent offline analysis of their immersion-freezing behavior.

3.3 Collection efficiency of atmospheric INPs

In addition to the experiments with conditioned particles in the laboratory, atmospheric particles were sampled with HERA to evaluate the new method for a mixture of particles of different sizes and chemical compositions. HALF-BAC was sampling in parallel to produce a benchmark for the comparison of retrieved INP concentrations. Both instruments were operated on the roof of the Cloud Laboratory at TROPOS, i.e., at near-standard pressure conditions, with their separate inlets oriented in the main wind direction. Both the HERA and HALFBAC inlets were equipped with conductive silicone tubing (inner diameter HERA: 17.4 mm, HALFBAC: 11.2 mm). Eight filter samples were collected from each instrument on several days in May, June, and Au-

gust 2020. Table 1 lists the date and time of the sampling periods including sampling volume, mean wind speed, and mean temperature as measured at the TROPOS weather station. The immersion INP analysis was performed with INDA for filters sampled on 28 May 2020 and with LINA for the remaining samples. Figure 7a aims to visualize the dependency of instrument agreement on the wind conditions during sampling. Root-mean-squared logarithmic errors (RMSLEs) of INP concentrations from HERA $N_{\mathrm{INP,HERA}}$ and HALFBAC $N_{\mathrm{INP,HALFBAC}}$ were determined according to Eq. (1), with n being the number of available, non-zero data points:

$$\mathrm{RMSLE} =$$

$$\sqrt{\frac{1}{n}\sum_{i=1}^{n}\left[\ln\left(1 + N_{\mathrm{INP,HERA}}\right) - \ln\left(1 + N_{\mathrm{INP,HALFBAC}}\right)\right]^{2}}. \quad (1)$$

RMSLE values are shown on the y axis and are contrasted with the variability in wind speed and direction during the different sampling periods. The single standard deviation in wind direction is shown on the x axis, whereas the single standard deviation in wind speed is represented by the marker size. This analysis was performed because HERA and HALFBAC were sampling from their individual inlets with different inner diameters. Calculations of the overall sampling efficiencies (aspiration and transmission) of HERA and HALFBAC performed with the Particle Loss Calculator (not shown) suggest strong effects of variations in wind speed and direction in the case of HALFBAC due to its smaller inner inlet diameter, while the HERA sampling efficiency is only slightly influenced by variable wind conditions. Overall, sampling is more efficient with HERA compared to HALFBAC in the size range from 0 to 8 μm, which comprises the vast majority of available aerosol particles (see coarse mode measurements by Mordas et al., 2015, for summer urban background aerosol). An increase in aspiration angle (0° if inlet is facing wind directly) and a decrease in wind speed cause particles to be sampled less efficiently with HALFBAC. To illustrate, D_{50} shifts from 10.4 μm (wind speed $3\,\mathrm{m\,s}^{-1}$, aspiration angle 0°) to 5.0 μm (wind speed $1\,\mathrm{m\,s}^{-1}$, aspiration angle 60°). Note that this only holds for the here-presented inlet configuration.

Regarding the measured INP concentrations, instrument agreement seems to decrease with an increase in wind direction variability, whereas no clear dependency on wind speed variability can be found for the eight sampling periods (see Fig. 7a). Sampling periods 3, 4, and 5 with high RMSLE values and high wind direction variability (single standard deviation $> 30°$) are also the ones with the lowest mean wind speed (1.4 to $1.7\,\mathrm{m\,s}^{-1}$; see Table 1). In this wind speed range with aspiration angles $> 0°$, sampling with HALFBAC was calculated to be significantly less efficient than sampling with HERA, which could account for the observed discrepancies in INP concentration. As a result, data points representing periods 3, 4, and 5 are colored grey, and INP spectra are not shown. Discrepancies in INP concentrations retrieved from filter samplers using different inlet configurations have also been observed by Lacher et al. (2023). In this study, filters from open-face filter samplers occasionally showed higher INP concentrations than filters sampled from a common total inlet, and observed differences sometimes coincided with a change in wind speed. Concerning the HERA and HALFBAC comparison during the remaining five sampling periods with steady wind direction and elevated wind speeds, we find very good agreement between the two samplers in both shape and magnitude of the INP spectra (see Fig. 7b, c, and d with the colors corresponding to those in Fig. 7a). INP concentrations retrieved from HERA filters are often slightly above those from HALFBAC, which is potentially related to the slightly more efficient sampling of the majority of the aerosol particle size distribution. In summary, INP concentrations agree within measurement uncertainty for the sampling periods that presumably did not feature significant differences in sampling efficiency between HERA and HALFBAC.

4 First results from aircraft sampling

As described in Sect. 1, a prototype of HERA was deployed on the Polar 5 aircraft of the Alfred Wegener Institute (AWI) during PAMARCMiP 2018. For this first test, one filter was sampled per flight at a flow rate of $10\,\mathrm{L\,min}^{-1}$ (Hartmann et al., 2020). Only afterwards was HERA equipped with the pump unit described earlier (see Sect. 2.1) to achieve higher flow rates. The first application of the upgraded HERA system was the HALO mission CIRRUS-HL in June and July 2021. For this, HERA was installed on HALO as shown in Fig. 1a, with sampling lines from both the HASI for sampling outside cloud aerosol particles and the HALO-CVI for sampling cloud particle residuals. Before installation, HERA was thoroughly tested for leaks in the laboratory by evacuation of the system and comparison of flow rates measured at the HERA inlet and the pump unit at low pressure. The HASI and the aerosol sampling line were revised prior to CIRRUS-HL in cooperation with Enviscope GmbH to enable more efficient sampling of supermicron aerosol particles at flow rates higher than $30\,\mathrm{L\,min}^{-1}$. Briefly, the setup was changed from several small diffusors within a main diffusor, each being connected to the instruments with their individual sampling lines (Minikin et al., 2017), to a single diffusor (inlet tip diameter 8.82 mm) connected to a main sampling line with larger inner diameter (15.75 mm). All instruments were connected to this main sampling line at individual junction points, with HERA sampling at the end of the line at a volumetric flow rate of $40\,\mathrm{L\,min}^{-1}$ (total length from HASI to HERA ~ 7 m). The total airflow was regulated according to the TAS via a bypass to ensure near-isokinetic sampling at all times. For example, $\sim 73\,\mathrm{L\,min}^{-1}$ was pulled through the inlet at $200\,\mathrm{m\,s}^{-1}$ (flight altitude of ~ 11 km). Furthermore, compensation pumps were installed to mini-

Table 1. Sampling periods for the comparison of INP concentrations from filters sampled with HERA and HALFBAC. The meteorological data were measured at the TROPOS weather station and averaged over the sampling period.

Sample ID	Date (yyyy-mm-dd)	Time start (UTC)	Time stop (UTC)	Volume (L)	Temperature (°C)	Wind speed (m s^{-1})
1	2020-05-28	09:03:00	11:33:00	4500	15.8	3.8
2	2020-05-28	12:54:00	15:24:00	4500	18.2	3.2
3	2020-06-02	07:40:00	10:10:00	4500	21.7	1.4
4	2020-06-02	10:52:00	13:22:00	4500	24.7	1.7
5	2020-08-06	12:25:00	15:05:00	4800	30.6	1.7
6	2020-08-11	08:15:00	10:44:00	4470	29.6	2.6
7	2020-08-11	12:45:00	14:15:00	2700	32.1	2.6
8	2020-08-12	08:32:00	11:02:00	4500	29.8	3.0
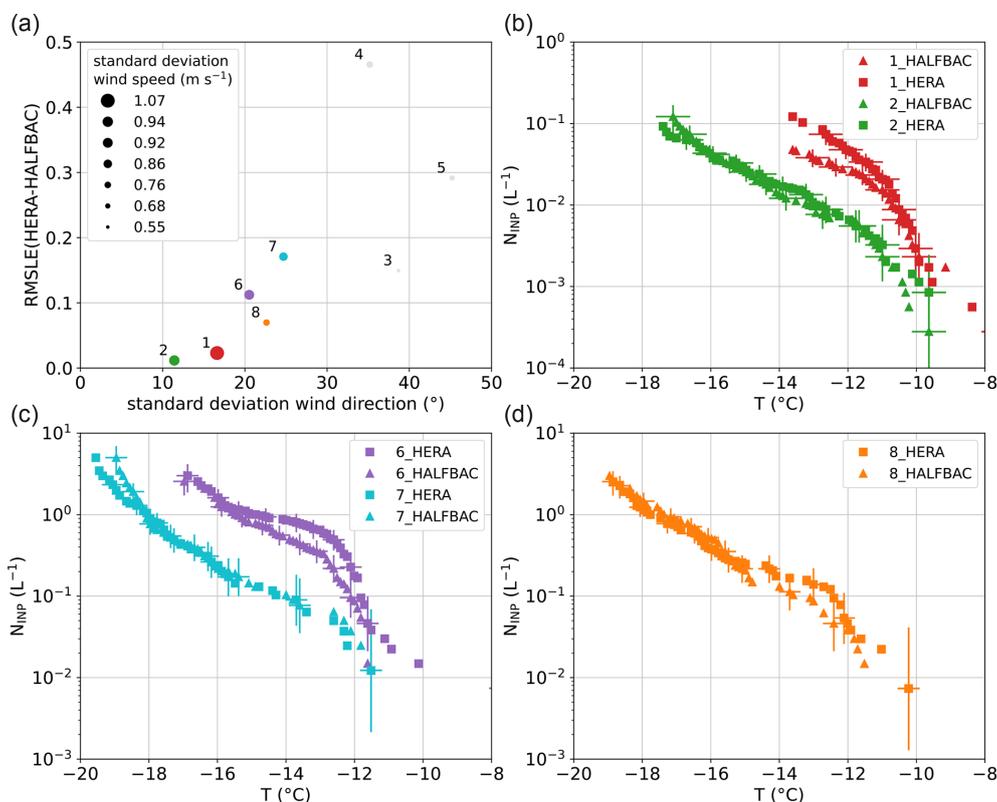
Figure 7. (a) RMSLE-based deviation between INP concentrations from the HERA and HALFBAC filters with respect to the variability in wind direction during the sampling periods. Note that for this only the temperature range was used where non-zero data from both instruments were available. The marker size refers to the variability in wind speed. Colored data points correspond to the INP spectra shown panels **(b)**, **(c)**, and **(d)**. Grey data points indicate sampling periods with high variability in wind direction and low wind speeds for which the INP spectra were not further analyzed. **(b–d)** INP concentrations (N_{INP}) from filter samples collected with HERA (squares) and HALFBAC (triangles) with respect to temperature.

mize variations in the total flow rate when the HERA pumps were not running. In comparison to the mere consideration of the HERA geometry (see Fig. 2), the sampling efficiency of supermicron particles was significantly reduced during CIRRUS-HL. This is due to the connection of HERA to two inlets, which resulted in rather long sampling lines featuring several bends and leading to an increase in sedimenta-

tion and impaction losses. Assuming spherical particles with a density of 2 g cm^{-1}, an inline pressure of 340 mbar, and an inline temperature of 26 °C (corresponding to $\sim$200 m s^{-1} TAS), D_{50} at the HASI is 2.7 µm (aspiration and transmission efficiency). The HALO-CVI sampling line to HERA had a total length of $\sim$5 m (10 mm inner diameter until flow distribution at roughly half of total length, then contraction

to 4.57 mm), resulting in $D_{50} = 2.2\,\mu\text{m}$ for the above-given conditions ($D_{50} = 4.7\,\mu\text{m}$ from HALO-CVI inlet to flow distribution). The volumetric flow rate of HERA at the HALO-CVI was $\sim 5\,\text{L min}^{-1}$ which is due to the inlet-specific restriction of total flow rate. However, since cloud particles and hence residuals are enriched in the HALO-CVI, the lower flow rate does not decrease the probability to collect INPs in comparison to sampling at the HASI. Note that the HALO-CVI aspires cloud particles in a size range from ~ 5 to $\sim 60\,\mu\text{m}$ from which liquid water/ice is evaporated/sublimated to release the cloud particle residuals (Seifert et al., 2004; Twohy and Poellot, 2005).

Figure 8 shows frozen fractions with respect to temperature retrieved from LINA measurements of three sampled filters and one blank of research flight (RF) 15 of CIRRUS-HL on 13 July 2021. See Appendix A for details concerning the immersion INP analysis. The filters sampled at the HASI are shown in red and green, the filter sampled at the HALO-CVI is shown in blue, and the blank is shown in grey. The HERA inlet pressure during sampling ranged between 1030 and 220 mbar. The average cabin pressure was ~ 800 mbar. The background of the ultrapure water (light blue area in Fig. 8) represents the upper and lower limits including uncertainty from six measurements. On the one hand, it can be seen that the blank is close to the ultrapure water background, indicating that only very few additional INPs were introduced due to filter handling and storage in HERA. The filters sampled at the HASI and HALO-CVI, on the other hand, show significantly higher onset freezing temperatures than the blank and the ultrapure water. All droplets are frozen at $-28\,°\text{C}$, while the frozen fraction is only $\sim 30\,\%$ in the case of the blank filter at the same temperature. The vast majority of INPs sampled on the filters must hence stem from the air collected through the aircraft inlets. The frozen fraction measurements of the HASI and HALO-CVI filter samples show distinct features indicating that different INP populations with specific immersion-freezing properties have been collected. While the discussion of these features is beyond the scope of this study, the observed differences between samples are suggestive of the sensitivity of the HERA filter samples with respect to variations of atmospheric INP concentrations. To summarize, also at low inline pressure, there is neither a noticeable cross-contamination between the HERA filter samples nor a significant contamination from filter handling or leaks between HERA and the pressurized cabin.

5 Summary and outlook

In this paper, we introduced the new High-volume flow aERosol particle filter sAmpler (HERA) for aircraft applications. HERA can be equipped with up to six filters, with in-flight filter changes realized with the help of an electrically driven valve. The powerful actively controlled pump
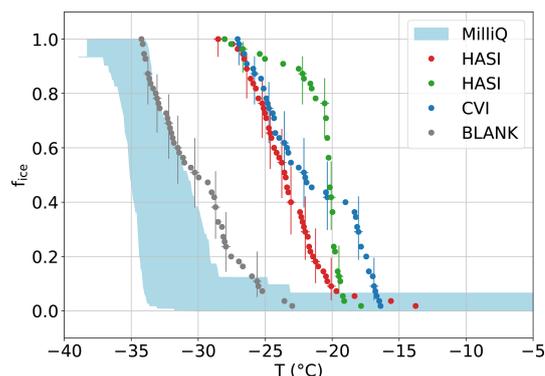
Figure 8. Frozen fraction (f_{ice}) with respect to temperature from RF 15 of CIRRUS-HL measured with LINA. Aerosol particle filters sampled at the HASI are shown in red and green, a cloud particle residual filter sampled at the HALO-CVI is shown in blue, and a blank filter is shown in grey. The ultrapure water background (Milli-Q) is shown in light blue in the background and represents the upper and lower limits of six water measurements including the measurement uncertainty.

unit enables sampling at a flow rate exceeding $100\,\text{L min}^{-1}$, depending on the filter medium and pressure conditions. The system was designed for efficient sampling of supermicron particles at high flow rates (particle transmission in HERA: $D_{50} = 7\,\mu\text{m}$ at $40\,\text{L min}^{-1}$ and near-standard pressure, exemplary particle transmission including aircraft inlet and sampling lines: $D_{50} = 2.7\,\mu\text{m}$ at $40\,\text{L min}^{-1}$ and 340 mbar). These features make HERA highly automatable, minimize the risk of contamination, and enable high temporal and spatial resolutions for INP concentration measurements.

Proof of principle experiments with SNOMAX® and ATD were conducted. For this, particles were generated from a suspension, size-selected (300, 500, and 800 nm), and sampled at different flow rates (10, 40, and $100\,\text{L min}^{-1}$) onto filters with HERA, followed by rinsing of the filters to generate a suspension for immersion INP analysis. We did observe good agreement for the ice-nucleation-active site density per SNOMAX® mass and ATD surface area in comparison to literature results (Polen et al., 2016; Perkins et al., 2019), where suspensions were directly used for immersion INP analysis. Furthermore, no dependency of particle size or flow rate on the results of the immersion INP analysis was found, which is in accordance with the theoretical particle transmission calculations. These findings suggest efficient sampling of INPs without any alteration of their immersion-freezing properties (e.g., due to storage of the filters or impaction of INPs on the filter surface) in the investigated parameter space.

The performance of HERA was compared to the more straightforward filter sampler HALFBAC by ground-based collection of atmospheric aerosol particles and analysis of their immersion-freezing behavior. A dependency of the difference in INP concentration from HERA and HALFBAC on the mean wind speed and variability in wind direction during

the sampling periods was found. This effect was interpreted as being due to the lack of a common inlet and associated differences in sampling efficiency. The sampling efficiency was calculated to vary strongly in the case of HALFBAC, which had a smaller inlet inner diameter than HERA, with changes in wind speed and direction, while no strong effect could be seen for HERA. Filters from both instruments yielded similar results as long as periods with unfavorable wind conditions for sampling with HALFBAC were excluded.

During the CIRRUS-HL mission, HERA was operated on HALO for the first time. Results from RF 15, where three filters were sampled at HERA inlet pressure values between 1030 and 220 mbar, show a blank filter background close to the ultrapure water. The filters sampled at the HASI and HALO-CVI each featured distinct freezing spectra and ice nucleation activity significantly above the blank background. These results indicate the sensitivity of the immersion-freezing measurements of the HERA filter samples with respect to different atmospheric conditions. Furthermore, it can be concluded that no notable contamination was introduced via filter handling and leakage currents between filter holder pathways in HERA or between HERA and the pressurized aircraft cabin.

Future investigations will focus on the evaluation of the HERA filter samples from the HALO CIRRUS-HL mission with respect to the origin of the sampled air masses, aerosol particle and cloud particle residual size distributions, and particle chemical composition. In addition, HERA was operated on the AWI Polar 6 aircraft during HALO-(AC)[3] (Arctic Air Mass Transformations During Warm Air Intrusions And Marine Cold Air Outbreaks) in spring 2022 and BACSAM I (Boundary Layer and Atmospheric Aerosol- and Cloud Study) in fall 2022, and data are currently being evaluated. Setups for these campaigns have been, and upcoming ones will continue to be, planned in such a manner that sampling flow rates are maximized and hence temporal and spatial resolutions of retrieved INP concentrations further increased. Furthermore, we plan to investigate HERA filter extracts with alternative offline methods featuring lower background levels, e.g., microfluidics (Stan et al., 2009; Reicher et al., 2018; Tarn et al., 2018), to increase the measurable INP concentration range. The analysis of physicochemical properties of the collected aerosol particles other than their immersion-freezing behavior (see Sect. 1) will also be explored in the future.

So far, filter changes in HERA have been triggered by an on-board operator. For sampling in clouds and complex flight patterns, this cannot be avoided. However, it could be feasible to use information from other systems on the aircraft (geographical position, altitude, temperature, pressure, or others) as input parameters for the HERA software and trigger filter changes according to certain threshold values. This would enable the application of HERA on a more regular basis, e.g., on commercial aircraft or measurement campaigns with a very limited number of on-board operators. Additional

HERA systems could be produced for simultaneous integration on different aircraft. With this, the currently small set of free tropospheric INP concentration data could be expanded to further improve our understanding of the role of INPs on cloud formation and properties.

Appendix A: Offline immersion INP analysis

To evaluate the filters sampled with HERA, offline immersion INP measurement techniques are used. These are the Leipzig Ice Nucleation Array (LINA) and the Ice Nucleation Droplet Array (INDA). LINA is a cold-stage setup, where ninety 1 μL sized droplets of filter washing water are pipetted onto a hydrophobic glass slide (Paul Marienfeld GmbH & Co. KG, Germany) situated on a Peltier element. INDA operates with 50 μL sized aliquots in a 96-well PCR (polymerase chain reaction) tray (Brand GmbH & Co. KG, Germany) situated in an ethanol bath. In both cases, samples are being cooled down at a rate of $\sim 1\,\text{K\,min}^{-1}$. A filter extract is prepared by removing the filter from cold storage ($-20\,°\text{C}$), placing it into a centrifuge tube (50 mL, Greiner Bio-One GmbH, Germany) together with 3 mL of ultrapure water (Milli-Q, $18.2\,\text{M}\Omega\,\text{cm}^{-1}$), and agitating with a laboratory flask shaker for 15 min to wash off collected particles. After removing 100 μL for the LINA measurement, the centrifuge tube with the remaining sample is shaken again after adding another 3.1 mL of ultrapure water to supply a sufficient sample volume for the INDA measurement with the 96-well PCR tray. This standard method was applied to all measurements presented here unless otherwise stated. Both the LINA and INDA setups and temperature calibration routines have previously been described in detail (Chen et al., 2018; Hartmann et al., 2019). The temperature uncertainty of the here-presented data is $\pm 0.32\,\text{K}$ for LINA and $\pm 0.50\,\text{K}$ for INDA (single standard deviation of at least three calibration experiments). The uncertainty of the measured frozen fractions, i.e., the number of frozen droplets divided by the total number of droplets, is given as the 95 % binomial sampling confidence intervals (Agresti and Coull, 1998).

For the LINA measurements with samples from CIRRUS-HL (see Sect. 4), instead of hydrophobic glass slides, Si wafers (with (100) orientation, undoped, 50.8 mm; Si-Mat (Silicon Materials), Germany) were used as a substrate. In test measurements with ultrapure water, frozen fractions of an ensemble of 1 μL sized droplets tended to be significantly shifted towards lower temperatures when comparing the Si wafers to the hydrophobic glass slides (average shift of $-3\,\text{K}$ at a frozen fraction of 50 %). The temperature of the droplets on the Si wafers was calibrated using higher alkanes (n-undecane and n-tridecane, 99 %, Thermo Fisher Scientific Inc., USA) with defined melting points as described by Budke and Koop (2015). The temperature uncertainty was estimated to be $\pm 0.33\,\text{K}$ (single standard deviation of three individual measurements with both substances). In contrast

to the LINA measurements using glass slides, measurements were performed with 55 droplets instead of 90. This is due to the surface properties of the Si wafers for which droplets feature a smaller contact angle and thus spread out over a larger area in comparison to the hydrophobic glass slides. The total number of droplets hence had to be decreased to 55 to still fit on the cooling element of LINA.

Frozen fraction measurements from LINA and INDA can be combined via normalization with respect to different quantities. For example, one can calculate the INP concentration, i.e., normalizing the frozen fraction with the volume of sampled air; the volume of the washing water; and the droplet volume according to Vali (1971) as shown in Fig. 7. Other normalization methods are the number of INPs per filter (accounting for volume of washing water and droplet volume; see Fig. 4), the ice-nucleation-active site density per unit mass n_m (accounting for volume of the washing water, the droplet volume, and the particle mass per filter; see Fig. 5), and the ice-nucleation-active surface site density n_s (accounting for volume of the washing water, the droplet volume, and the particle surface area per filter; see Fig. 6).

Author contributions. The experiments were conceptualized by CJ, HW, and FS. The sampling experiments were performed by CJ, JS, HW, and SG. SM supported sampling behind the HALO-CVI during CIRRUS-HL and performed particle loss calculations for the HALO-CVI sampling line. SG performed the particle loss calculations for HERA and HALFBAC, and JS did so for the HASI inlet and sampling line. The immersion-freezing experiments were performed by JS and SG. The data evaluation and interpretation were performed by SG with contributions from JS, HW, and FS. SG wrote the manuscript with contributions from all co-authors.

References

Adams, M. P., Tarn, M. D., Sanchez-Marroquin, A., Porter, G. C. E., O'Sullivan, D., Harrison, A. D., Cui, Z., Vergara-Temprado, J., Carotenuto, F., Holden, M. A., Daily, M. I., Whale, T. F., Sikora, S. N. F., Burke, I. T., Shim, J.-U., McQuaid, J. B., and Murray, B. J.: A Major Combustion Aerosol Event Had a Negligible Impact on the Atmospheric Ice-Nucleating Particle Population, J. Geophys. Res.-Atmos., 125, e2020JD032938, https://doi.org/10.1029/2020JD032938, 2020.

Agresti, A. and Coull, B. A.: Approximate is better than "exact" for interval estimation of binomial proportions, Am. Stat., 52, 119–126, 1998.

Barry, K. R., Hill, T. C., Jentzsch, C., Moffett, B. F., Stratmann, F., and DeMott, P. J.: Pragmatic protocols for working cleanly when measuring ice nucleating particles, Atmos. Res., 250, 105419, https://doi.org/10.1016/j.atmosres.2020.105419, 2021a.

Barry, K. R., Hill, T. C. J., Levin, E. J. T., Twohy, C. H., Moore, K. A., Weller, Z. D., Toohey, D. W., Reeves, M., Campos, T., Geiss, R., Schill, G. P., Fischer, E. V., Kreidenweis, S. M., and DeMott, P. J.: Observations of Ice Nucleating Particles in the Free Troposphere From Western US Wildfires, J. Geophys. Res.-Atmos., 126, e2020JD033752, https://doi.org/10.1029/2020JD033752, 2021b.

Beall, C. M., Lucero, D., Hill, T. C., DeMott, P. J., Stokes, M. D., and Prather, K. A.: Best practices for precipitation sample storage for offline studies of ice nucleation in marine and coastal environments, Atmos. Meas. Tech., 13, 6473–6486, https://doi.org/10.5194/amt-13-6473-2020, 2020.

Bieber, P., Seifried, T. M., Burkart, J., Gratzl, J., Kasper-Giebl, A., Schmale III, D. G., and Grothe, H.: A drone-based bioaerosol sampling system to monitor ice nucleation particles in the lower atmosphere, Remote Sens., 12, 552, https://doi.org/10.3390/rs12030552, 2020.

Bigg, E. K.: Cross Sections of Ice Nucleus Concentrations at Altitude over Long Paths, J. Atmos. Sci., 24, 226–229, https://doi.org/10.1175/1520-0469(1967)024<0226:CSOINC>2.0.CO;2, 1967.

Borys, R. D.: Studies of ice nucleation by Arctic aerosol on AGASP-II, J. Atmos. Chem., 9, 169–185, 1989.

Brockmann, J. E.: Aerosol Transport in Sampling Lines and Inlets, Chap. 6, John Wiley & Sons, Ltd, 68–105, https://doi.org/10.1002/9781118001684.ch6, 2011.

Budke, C. and Koop, T.: BINARY: an optical freezing array for assessing temperature and time dependence of heterogeneous ice nucleation, Atmos. Meas. Tech., 8, 689–703, https://doi.org/10.5194/amt-8-689-2015, 2015.

Burton, N. C., Grinshpun, S. A., and Reponen, T.: Physical collection efficiency of filter materials for bacteria and viruses, Ann. Occup. Hyg., 51, 143–151, 2007.

Chen, J., Wu, Z., Augustin-Bauditz, S., Grawe, S., Hartmann, M., Pei, X., Liu, Z., Ji, D., and Wex, H.: Ice-nucleating particle concentrations unaffected by urban air pollution in Beijing, China, Atmos. Chem. Phys., 18, 3523–3539, https://doi.org/10.5194/acp-18-3523-2018, 2018.

Coluzza, I., Creamean, J., Rossi, M. J., Wex, H., Alpert, P. A., Bianco, V., Boose, Y., Dellago, C., Felgitsch, L., Fröhlich-Nowoisky, J., Herrmann, H., Jungblut, S., Kanji, Z. A., Menzl, G., Moffett, B., Moritz, C., Mutzel, A., Pöschl, U., Schauperl, M., Scheel, J., Stopelli, E., Stratmann, F., Grothe, H., and Schmale, D. G.: Perspectives on the Future of Ice Nucleation Research: Research Needs and Unanswered Questions Identified from Two International Workshops, Atmosphere, 8, 138, https://doi.org/10.3390/atmos8080138, 2017.

Conen, F., Henne, S., Morris, C. E., and Alewell, C.: Atmospheric ice nucleators active $\geq -12\,°C$ can be quantified on PM_{10} filters, Atmos. Meas. Tech., 5, 321–327, https://doi.org/10.5194/amt-5-321-2012, 2012.

Conen, F., Einbock, A., Mignani, C., and Hüglin, C.: Measurement report: Ice-nucleating particles active $\geq -15\,°C$ in free tropospheric air over western Europe, Atmos. Chem. Phys., 22, 3433–3444, https://doi.org/10.5194/acp-22-3433-2022, 2022.

Connolly, P. J., Möhler, O., Field, P. R., Saathoff, H., Burgess, R., Choularton, T., and Gallagher, M.: Studies of heterogeneous freezing by three different desert dust samples, Atmos. Chem. Phys., 9, 2805–2824, https://doi.org/10.5194/acp-9-2805-2009, 2009.

Creamean, J. M., Suski, K. J., Rosenfeld, D., Cazorla, A., DeMott, P. J., Sullivan, R. C., White, A. B., Ralph, F. M., Minnis, P., Comstock, J. M., Tomlinson, J. M., and Prather, K. A.: Dust and Biological Aerosols from the Sahara and Asia Influence Precipitation in the Western U.S., Science, 339, 1572–1578, https://doi.org/10.1126/science.1227279, 2013.

Creamean, J. M., Primm, K. M., Tolbert, M. A., Hall, E. G., Wendell, J., Jordan, A., Sheridan, P. J., Smith, J., and Schnell, R. C.: HOVERCAT: a novel aerial system for evaluation of aerosol–cloud interactions, Atmos. Meas. Tech., 11, 3969–3985, https://doi.org/10.5194/amt-11-3969-2018, 2018.

Cwiertny, D. M., Baltrusaitis, J., Hunter, G. J., Laskin, A., Scherer, M. M., and Grassian, V. H.: Characterization and acid-mobilization study of iron-containing mineral dust source materials, J. Geophys. Res.-Atmos., 113, D05202, https://doi.org/10.1029/2007JD009332, 2008.

DeMott, P. J., Cziczo, D. J., Prenni, A. J., Murphy, D. M., Kreidenweis, S. M., Thomson, D. S., Borys, R., and Rogers, D. C.: Measurements of the concentration and composition of nuclei for cirrus formation, P. Natl. Acad. Sci. USA, 100, 14655–14660, 2003a.

DeMott, P. J., Sassen, K., Poellot, M. R., Baumgardner, D., Rogers, D. C., Brooks, S. D., Prenni, A. J., and Kreidenweis, S. M.: African dust aerosols as atmospheric ice nuclei, Geophys. Res. Lett., 30, 1732, https://doi.org/10.1029/2003GL017410, 2003b.

DeMott, P. J., Prenni, A. J., Liu, X., Kreidenweis, S. M., Petters, M. D., Twohy, C. H., Richardson, M. S., Eidhammer, T., and Rogers, D. C.: Predicting global atmospheric ice nuclei distributions and their impacts on climate, P. Natl. Acad. Sci. USA, 107, 11217–11222, 2010.

DeMott, P. J., Möhler, O., Stetzer, O., Vali, G., Levin, Z., Petters, M. D., Murakami, M., Leisner, T., Bundke, U., Klein, H., Kanji, Z. A., Cotton, R., Jones, H., Benz, S., Brinkmann, M., D., R., Saathoff, H., Nicolet, M., Saito, A., Nillius, B., Bingemer, H., Abbatt, J. P. D., Ardon, K., Ganor, E., Georgakopoulos, D. G., and Saunders, C. P. R.: Resurgence in ice nuclei measurement research, B. Am. Meteorol. Soc., 92, 1623–1635, 2011.

DeMott, P. J., Prenni, A. J., McMeeking, G. R., Sullivan, R. C., Petters, M. D., Tobo, Y., Niemand, M., Möhler, O., Snider, J. R., Wang, Z., and Kreidenweis, S. M.: Integrating laboratory and field data to quantify the immersion freezing ice nucleation activity of mineral dust particles, Atmos. Chem. Phys., 15, 393–409, https://doi.org/10.5194/acp-15-393-2015, 2015.

DeMott, P. J., Hill, T. C. J., McCluskey, C. S., Prather, K. A., Collins, D. B., Sullivan, R. C., Ruppel, M. J., Mason, R. H., Irish, V. E., Lee, T., Hwang, C. Y., Rhee, T. S., Snider, J. R., McMeeking, G. R., Dhaniyala, S., Lewis, E. R., Wentzell, J. J. B., Abbatt, J., Lee, C., Sultana, C. M., Ault, A. P., Axson, J. L., Diaz Martinez, M., Venero, I., Santos-Figueroa, G., Stokes, M. D., Deane, G. B., Mayol-Bracero, O. L., Grassian, V. H., Bertram, T. H., Bertram, A. K., Moffett, B. F., and Franc, G. D.: Sea spray aerosol as a unique source of ice nucleating particles, P. Natl. Acad. Sci. USA, 113, 5797–5803, 2016.

DeMott, P. J., Möhler, O., Cziczo, D. J., Hiranuma, N., Petters, M. D., Petters, S. S., Belosi, F., Bingemer, H. G., Brooks, S. D., Budke, C., Burkert-Kohn, M., Collier, K. N., Danielczok, A., Eppers, O., Felgitsch, L., Garimella, S., Grothe, H., Herenz, P., Hill, T. C. J., Höhler, K., Kanji, Z. A., Kiselev, A., Koop, T., Kristensen, T. B., Krüger, K., Kulkarni, G., Levin, E. J. T., Murray, B. J., Nicosia, A., O'Sullivan, D., Peckhaus, A., Polen, M. J., Price, H. C., Reicher, N., Rothenberg, D. A., Rudich, Y., Santachiara, G., Schiebel, T., Schrod, J., Seifried, T. M., Stratmann, F., Sullivan, R. C., Suski, K. J., Szakáll, M., Taylor, H. P., Ullrich, R., Vergara-Temprado, J., Wagner, R., Whale, T. F., Weber, D., Welti, A., Wilson, T. W., Wolf, M. J., and Zenker, J.: The Fifth International Workshop on Ice Nucleation phase 2 (FIN-02): laboratory intercomparison of ice nucleation measurements, Atmos. Meas. Tech., 11, 6231–6257, https://doi.org/10.5194/amt-11-6231-2018, 2018.

Fitzner, M., Pedevilla, P., and Michaelides, A.: Predicting heterogeneous ice nucleation with a data-driven approach, Nat. Commun., 11, 4777, https://doi.org/10.1038/s41467-020-18605-3, 2020.

Flyger, H., Hansen, K., Megaw, W. J., and Cox, L. C.: The Background Level of the Summer Tropospheric Aerosol Over Greenland and the North Atlantic Ocean, J. Appl. Meteorol. Clim., 12, 161–174, https://doi.org/10.1175/1520-0450(1973)012<0161:TBLOTS>2.0.CO;2, 1973.

Forster, P., Storelvmo, T., Armour, K., Collins, W., Dufresne, J.-L., Frame, D., Lunt, D., Mauritsen, T., Palmer, M., Watanabe, M., Wild, M., and Zhang, H.: The Earth's Energy Budget, Climate Feedbacks, and Climate Sensitivity, Cambridge University Press, Cambridge, United Kingdom and New York, NY, USA, 923–1054, https://doi.org/10.1017/9781009157896.009, 2021.

Garimella, S., Kristensen, T. B., Ignatius, K., Welti, A., Voigtländer, J., Kulkarni, G. R., Sagan, F., Kok, G. L., Dorsey, J., Nichman, L., Rothenberg, D. A., Rösch, M., Kirchgäßner, A. C. R., Ladkin, R., Wex, H., Wilson, T. W., Ladino, L. A., Abbatt, J.

P. D., Stetzer, O., Lohmann, U., Stratmann, F., and Cziczo, D. J.: The SPectrometer for Ice Nuclei (SPIN): an instrument to investigate ice nucleation, Atmos. Meas. Tech., 9, 2781–2795, https://doi.org/10.5194/amt-9-2781-2016, 2016.

Grawe, S., Jentzsch, C., Schaefer, J., Wex, H., Mertes, S., and Stratmann, F.: Data for figures in "Next-generation ice nucleating particle sampling on aircraft: Characterization of the High-volume flow aERosol particle filter sAmpler (HERA)", Zenodo [data set], https://doi.org/10.5281/zenodo.8309936, 2023.

Hartmann, M., Blunier, T., Brügger, S., Schmale, J., Schwikowski, M., Vogel, A., Wex, H., and Stratmann, F.: Variation of Ice Nucleating Particles in the European Arctic Over the Last Centuries, Geophys. Res. Lett., 46, 4007–4016, https://doi.org/10.1029/2019GL082311, 2019.

Hartmann, M., Adachi, K., Eppers, O., Haas, C., Herber, A., Holzinger, R., Hünerbein, A., Jäkel, E., Jentzsch, C., van Pinxteren, M., Wex, H., Willmes, S., and Stratmann, F.: Wintertime Airborne Measurements of Ice Nucleating Particles in the High Arctic: A Hint to a Marine, Biogenic Source for Ice Nucleating Particles, Geophys. Res. Lett., 47, e2020GL087770, https://doi.org/10.1029/2020GL087770, 2020.

Hartmann, M., Gong, X., Kecorius, S., van Pinxteren, M., Vogl, T., Welti, A., Wex, H., Zeppenfeld, S., Herrmann, H., Wiedensohler, A., and Stratmann, F.: Terrestrial or marine – indications towards the origin of ice-nucleating particles during melt season in the European Arctic up to 83.7° N, Atmos. Chem. Phys., 21, 11613–11636, https://doi.org/10.5194/acp-21-11613-2021, 2021.

Hill, T., DeMott, P., Conen, F., and Möhler, O.: Impacts of Bioaerosols on Atmospheric Ice Nucleation Processes, Chap. 3.1, 195–219, John Wiley & Sons, Ltd, https://doi.org/10.1002/9781119132318.ch3a, 2017.

Hill, T. C., Moffett, B. F., DeMott, P. J., Georgakopoulos, D. G., Stump, W. L., and Franc, G. D.: Measurement of ice nucleation-active bacteria on plants and in precipitation by quantitative PCR, Appl. Environ. Microb., 80, 1256–1267, 2014.

Irish, V. E., Elizondo, P., Chen, J., Chou, C., Charette, J., Lizotte, M., Ladino, L. A., Wilson, T. W., Gosselin, M., Murray, B. J., Polishchuk, E., Abbatt, J. P. D., Miller, L. A., and Bertram, A. K.: Ice-nucleating particles in Canadian Arctic sea-surface microlayer and bulk seawater, Atmos. Chem. Phys., 17, 10583–10595, https://doi.org/10.5194/acp-17-10583-2017, 2017.

Jakobsson, J. K. F., Waman, D. B., Phillips, V. T. J., and Bjerring Kristensen, T.: Time dependence of heterogeneous ice nucleation by ambient aerosols: laboratory observations and a formulation for models, Atmos. Chem. Phys., 22, 6717–6748, https://doi.org/10.5194/acp-22-6717-2022, 2022.

Jimenez-Sanchez, C., Hanlon, R., Aho, K. A., Powers, C., Morris, C. E., and Schmale III, D. G.: Diversity and ice nucleation activity of microorganisms collected with a small unmanned aircraft system (sUAS) in France and the United States, Front. Microbiol., 9, https://doi.org/10.3389/fmicb.2018.01667, 2018.

Joly, M., Amato, P., Deguillaume, L., Monier, M., Hoose, C., and Delort, A.-M.: Quantification of ice nuclei active at near 0 °C temperatures in low-altitude clouds at the Puy de Dôme atmospheric station, Atmos. Chem. Phys., 14, 8185–8195, https://doi.org/10.5194/acp-14-8185-2014, 2014.

Knackstedt, K., Moffett, B. F., Hartmann, S., Wex, H., Hill, T. C. J., Glasgo, E., Reitz, L., Augustin-Bauditz, S., Beall, B., Bullerjahn, G. S., Fröhlich-Nowoisky, J., Grawe, S., Lubitz, J., Stratmann,

F., and McKay, R. M.: A terrestrial origin for abundant riverine nanoscale ice-nucleating particles, Environ. Sci. Technol., 52, 12358–12367, 2018.

Kwiezinski, C., Weller, C., van Pinxteren, D., Brüggemann, M., Mertes, S., Stratmann, F., and Herrmann, H.: Determination of highly polar compounds in atmospheric aerosol particles at ultra-trace levels using ion chromatography Orbitrap mass spectrometry, J. Sep. Sci., 44, 2343–2357, https://doi.org/10.1002/jssc.202001048, 2021.

Lacher, L., DeMott, P. J., Levin, E. J. T., Suski, K. J., Boose, Y., Zipori, A., Herrmann, E., Bukowiecki, N., Steinbacher, M., Gute, E., Abbatt, J. P. D., Lohmann, U., and Kanji, Z. A.: Background Free-Tropospheric Ice Nucleating Particle Concentrations at Mixed-Phase Cloud Conditions, J. Geophys. Res.-Atmos., 123, 10506–10525, 2018.

Lacher, L., Adams, M. P., Barry, K., Bertozzi, B., Bingemer, H., Boffo, C., Bras, Y., Büttner, N., Castarede, D., Cziczo, D. J., DeMott, P. J., Fösig, R., Goodell, M., Höhler, K., Hill, T. C. J., Jentzsch, C., Ladino, L. A., Levin, E. J. T., Mertes, S., Möhler, O., Moore, K. A., Murray, B. J., Nadolny, J., Pfeuffer, T., Picard, D., Ramírez-Romero, C., Ribeiro, M., Richter, S., Schrod, J., Sellegri, K., Stratmann, F., Swanson, B. E., Thomson, E., Wex, H., Wolf, M., and Freney, E.: The Puy de Dôme ICe Nucleation Intercomparison Campaign (PICNIC): Comparison between online and offline methods in ambient air, EGUsphere [preprint], https://doi.org/10.5194/egusphere-2023-1125, 2023.

Levin, E. J., DeMott, P. J., Suski, K. J., Boose, Y., Hill, T. C., McCluskey, C. S., Schill, G. P., Rocci, K., Al-Mashat, H., Kristensen, L. J., Cornwell, G., Prather, K., Tomlinson, J., Mei, F., Hubbe, J., Pekour, M., Sullivan, R., Leung, L. R., and Kreidenweis, S. M.: Characteristics of Ice Nucleating Particles in and Around California Winter Storms, J. Geophys. Res.-Atmos., 124, 11530–11551, https://doi.org/10.1029/2019JD030831, 2019.

Lin, Y., Fan, J., Li, P., Leung, L.-R., DeMott, P. J., Goldberger, L., Comstock, J., Liu, Y., Jeong, J.-H., and Tomlinson, J.: Modeling impacts of ice-nucleating particles from marine aerosols on mixed-phase orographic clouds during 2015 ACAPEX field campaign, Atmos. Chem. Phys., 22, 6749–6771, https://doi.org/10.5194/acp-22-6749-2022, 2022.

Lindow, S. E.: Membrane fluidity as a factor in production and stability of bacterial ice nuclei active at high subfreezing temperatures, Cryobiology, 32, 247–258, 1995.

Liu, B. Y. H. and Lee, K. W.: Efficiency of membrane and nuclepore filters for submicrometer aerosols, Environ. Sci. Technol., 10, 345–350, https://doi.org/10.1021/es60115a002, 1976.

Maki, L. R., Galyan, E. L., Chang-Chien, M.-M., and Caldwell, D. R.: Ice Nucleation Induced by Pseudomonas syringae, Appl. Microbiol., 28, 456–459, https://doi.org/10.1128/am.28.3.456-459.1974, 1974.

Mason, R. H., Si, M., Chou, C., Irish, V. E., Dickie, R., Elizondo, P., Wong, R., Brintnell, M., Elsasser, M., Lassar, W. M., Pierce, K. M., Leaitch, W. R., MacDonald, A. M., Platt, A., Toom-Sauntry, D., Sarda-Estève, R., Schiller, C. L., Suski, K. J., Hill, T. C. J., Abbatt, J. P. D., Huffman, J. A., DeMott, P. J., and Bertram, A. K.: Size-resolved measurements of ice-nucleating particles at six locations in North America and one in Europe, Atmos. Chem. Phys., 16, 1637–1651, https://doi.org/10.5194/acp-16-1637-2016, 2016.

McCluskey, C. S., Hill, T. C. J., Humphries, R. S., Rauker, A. M., Moreau, S., Strutton, P. G., Chambers, S. D., Williams, A. G., McRobert, I., Ward, J., Keywood, M. D., Harnwell, J., Ponsonby, W., Loh, Z. M., Krummel, P. B., Protat, A., Kreidenweis, S. M., and DeMott, P. J.: Observations of Ice Nucleating Particles Over Southern Ocean Waters, Geophys. Res. Lett., 45, 11989–11997, https://doi.org/10.1029/2018GL079981, 2018.

Mertes, S., Verheggen, B., Walter, S., Connolly, P., Ebert, M., Schneider, J., Bower, K. N., Cozic, J., Weinbruch, S., Baltensperger, U., and Weingartner, E.: Counterflow Virtual Impactor Based Collection of Small Ice Particles in Mixed-Phase Clouds for the Physico-Chemical Characterization of Tropospheric Ice Nuclei: Sampler Description and First Case Study, Aerosol Sci. Tech., 41, 848–864, https://doi.org/10.1080/02786820701501881, 2007.

Michaud, A. B., Dore, J. E., Leslie, D., Lyons, W. B., Sands, D. C., and Priscu, J. C.: Biological ice nucleation initiates hailstone formation, J. Geophys. Res.-Atmos., 119, 12186–12197, https://doi.org/10.1002/2014JD022004, 2014.

Minikin, A., Sauer, D., Ibrahim, A., Franke, H., Röschenthaler, T., Fütterer, D. A., and Petzold, A.: The HALO Submicrometer Aerosol Inlet (HASI): Design concept and first characterization, German Aerospace Center, https://elib.dlr.de/116282/ (last access: 9 October 2023), 2017.

Moffett, B. F.: Fresh water ice nuclei, Fund. Appl. Limnol., 188, 19–23, 2016.

Mordas, G., Prokopciuk, N., Byčenkienė, S., Andriejauskienė, J., and Ulevicius, V.: Optical properties of the urban aerosol particles obtained from ground based measurements and satellite-based modelling studies, Adv. Meteorol., 2015, 898376, https://doi.org/10.1155/2015/898376, 2015.

Murray, B. J., Carslaw, K. S., and Field, P. R.: Opinion: Cloud-phase climate feedback and the importance of ice-nucleating particles, Atmos. Chem. Phys., 21, 665–679, https://doi.org/10.5194/acp-21-665-2021, 2021.

Ogren, J. A., Heintzenberg, J., and Charlson, R. J.: In-situ sampling of clouds with a droplet to aerosol converter, Geophys. Res. Lett., 12, 121–124, https://doi.org/10.1029/GL012i003p00121, 1985.

Peckhaus, A., Kiselev, A., Hiron, T., Ebert, M., and Leisner, T.: A comparative study of K-rich and Na/Ca-rich feldspar ice-nucleating particles in a nanoliter droplet freezing assay, Atmos. Chem. Phys., 16, 11477–11496, https://doi.org/10.5194/acp-16-11477-2016, 2016.

Perkins, R. J., Gillette, S. M., Hill, T. C., and DeMott, P. J.: The labile nature of ice nucleation by Arizona Test Dust, ACS Earth and Space Chemistry, 4, 133–141, 2019.

Petters, M. D. and Wright, T. P.: Revisiting ice nucleation from precipitation samples, Geophys. Res. Lett., 42, 8758–8766, 2015.

Phillips, V. T. J., DeMott, P. J., Andronache, C., Pratt, K. A., Prather, K. A., Subramanian, R., and Twohy, C.: Improvements to an Empirical Parameterization of Heterogeneous Ice Nucleation and Its Comparison with Observations, J. Atmos. Sci., 70, 378–409, https://doi.org/10.1175/JAS-D-12-080.1, 2013.

Polen, M., Lawlis, E., and Sullivan, R. C.: The unstable ice nucleation properties of Snomax® bacterial particles, J. Geophys. Res.-Atmos., 121, 11666–11678, 2016.

Polen, M., Brubaker, T., Somers, J., and Sullivan, R. C.: Cleaning up our water: reducing interferences from nonhomogeneous freezing of "pure" water in droplet freezing assays of ice-nucleating particles, Atmos. Meas. Tech., 11, 5315–5334, https://doi.org/10.5194/amt-11-5315-2018, 2018.

Porter, G. C. E., Sikora, S. N. F., Adams, M. P., Proske, U., Harrison, A. D., Tarn, M. D., Brooks, I. M., and Murray, B. J.: Resolving the size of ice-nucleating particles with a balloon deployable aerosol sampler: the SHARK, Atmos. Meas. Tech., 13, 2905–2921, https://doi.org/10.5194/amt-13-2905-2020, 2020.

Price, H. C., Baustian, K. J., McQuaid, J. B., Blyth, A., Bower, K. N., Choularton, T., Cotton, R. J., Cui, Z., Field, P. R., Gallagher, M., Hawker, R., Merrington, A., Miltenberger, A., Neely III, R. R., Parker, S. T., Rosenberg, P. D., Taylor, J. W., Trembath, J., Vergara-Temprado, J., Whale, T. F., Wilson, T. W., Young, G., and Murray, B. J.: Atmospheric Ice-Nucleating Particles in the Dusty Tropical Atlantic, J. Geophys. Res.-Atmos., 123, 2175–2193, https://doi.org/10.1002/2017JD027560, 2018.

Pruppacher, H. R. and Klett, J. D.: Microphysics of Clouds and Precipitation, Kluwer Academic Publishers, Dodrecht, the Netherlands, https://doi.org/10.1007/978-0-306-48100-0, 1997.

Pummer, B. G., Bauer, H., Bernardi, J., Bleicher, S., and Grothe, H.: Suspendable macromolecules are responsible for ice nucleation activity of birch and conifer pollen, Atmos. Chem. Phys., 12, 2541–2550, https://doi.org/10.5194/acp-12-2541-2012, 2012.

Reicher, N., Segev, L., and Rudich, Y.: The WeIzmann Supercooled Droplets Observation on a Microarray (WISDOM) and application for ambient dust, Atmos. Meas. Tech., 11, 233–248, https://doi.org/10.5194/amt-11-233-2018, 2018.

Reicher, N., Budke, C., Eickhoff, L., Raveh-Rubin, S., Kaplan-Ashiri, I., Koop, T., and Rudich, Y.: Size-dependent ice nucleation by airborne particles during dust events in the eastern Mediterranean, Atmos. Chem. Phys., 19, 11143–11158, https://doi.org/10.5194/acp-19-11143-2019, 2019.

Riechers, B., Wittbracht, F., Hütten, A., and Koop, T.: The homogeneous ice nucleation rate of water droplets produced in a microfluidic device and the role of temperature uncertainty, Phys. Chem. Chem. Phys., 15, 5873–5887, https://doi.org/10.1039/C3CP42437E, 2013.

Rogers, D. C.: Development of a continuous flow thermal gradient diffusion chamber for ice nucleation studies, Atmos. Res., 22, 149–181, 1988.

Rogers, D. C., DeMott, P. J., Kreidenweis, S. M., and Chen, Y.: Measurements of ice nucleating aerosols during SUCCESS, Geophys. Res. Lett., 25, 1383–1386, 1998.

Rogers, D. C., DeMott, P. J., and Kreidenweis, S. M.: Airborne measurements of tropospheric ice-nucleating aerosol particles in the Arctic spring, J. Geophys. Res.-Atmos., 106, 15053–15063, https://doi.org/10.1029/2000JD900790, 2001.

Rohatgi, A.: Webplotdigitizer: Version 4.6, https://automeris.io/WebPlotDigitizer (last access: 9 October 2023), 2022.

Sanchez-Marroquin, A., Hedges, D. H. P., Hiscock, M., Parker, S. T., Rosenberg, P. D., Trembath, J., Walshaw, R., Burke, I. T., McQuaid, J. B., and Murray, B. J.: Characterisation of the filter inlet system on the FAAM BAe-146 research aircraft and its use for size-resolved aerosol composition measurements, Atmos. Meas. Tech., 12, 5741–5763, https://doi.org/10.5194/amt-12-5741-2019, 2019.

Sanchez-Marroquin, A., Arnalds, O., Baustian-Dorsi, K. J., Browse, J., Dagsson-Waldhauserova, P., Harrison, A. D., Maters, E. C., Pringle, K. J., Vergara-Temprado, J., Burke, I. T., McQuaid, J. B., Carslaw, K. S., and Murray, B. J.: Ice-

land is an episodic source of atmospheric ice-nucleating particles relevant for mixed-phase clouds, Sci. Adv., 6, eaba8137, https://doi.org/10.1126/sciadv.aba8137, 2020.

Sanchez-Marroquin, A., West, J. S., Burke, I. T., McQuaid, J. B., and Murray, B. J.: Mineral and biological ice-nucleating particles above the South East of the British Isles, Environ. Sci.: Atmos., 1, 176–191, https://doi.org/10.1039/D1EA00003A, 2021.

Šantl-Temkiv, T., Amato, P., Gosewinkel, U., Thyrhaug, R., Charton, A., Chicot, B., Finster, K., Bratbak, G., and Löndahl, J.: High-flow-rate impinger for the study of concentration, viability, metabolic activity, and ice nucleation activity of airborne bacteria, Environ. Sci. Technol., 51, 11224–11234, https://doi.org/10.1021/acs.est.7b01480, 2017.

Schmid, D., Pridmore, D., Capitani, G., Battistutta, R., Neeser, J.-R., and Jann, A.: Molecular organisation of the ice nucleation protein InaV from Pseudomonas syringae, FEBS Lett., 414, 590–594, https://doi.org/10.1016/S0014-5793(97)01079-X, 1997.

Schneider, J., Höhler, K., Heikkilä, P., Keskinen, J., Bertozzi, B., Bogert, P., Schorr, T., Umo, N. S., Vogel, F., Brasseur, Z., Wu, Y., Hakala, S., Duplissy, J., Moisseev, D., Kulmala, M., Adams, M. P., Murray, B. J., Korhonen, K., Hao, L., Thomson, E. S., Castarède, D., Leisner, T., Petäjä, T., and Möhler, O.: The seasonal cycle of ice-nucleating particles linked to the abundance of biogenic aerosol in boreal forests, Atmos. Chem. Phys., 21, 3899–3918, https://doi.org/10.5194/acp-21-3899-2021, 2021.

Schrod, J., Weber, D., Drücke, J., Keleshis, C., Pikridas, M., Ebert, M., Cvetković, B., Nickovic, S., Marinou, E., Baars, H., Ansmann, A., Vrekoussis, M., Mihalopoulos, N., Sciare, J., Curtius, J., and Bingemer, H. G.: Ice nucleating particles over the Eastern Mediterranean measured by unmanned aircraft systems, Atmos. Chem. Phys., 17, 4817–4835, https://doi.org/10.5194/acp-17-4817-2017, 2017.

Schrod, J., Thomson, E. S., Weber, D., Kossmann, J., Pöhlker, C., Saturno, J., Ditas, F., Artaxo, P., Clouard, V., Saurel, J.-M., Ebert, M., Curtius, J., and Bingemer, H. G.: Long-term deposition and condensation ice-nucleating particle measurements from four stations across the globe, Atmos. Chem. Phys., 20, 15983–16006, https://doi.org/10.5194/acp-20-15983-2020, 2020.

Seifert, M., Ström, J., Krejci, R., Minikin, A., Petzold, A., Gayet, J.-F., Schlager, H., Ziereis, H., Schumann, U., and Ovarlez, J.: Aerosol-cirrus interactions: a number based phenomenon at all?, Atmos. Chem. Phys., 4, 293–305, https://doi.org/10.5194/acp-4-293-2004, 2004.

Seifried, T. M., Bieber, P., Kunert, A. T., Schmale, D. G., Whitmore, K., Fröhlich-Nowoisky, J., and Grothe, H.: Ice Nucleation Activity of Alpine Bioaerosol Emitted in Vicinity of a Birch Forest, Atmosphere, 12, 779, https://doi.org/10.3390/atmos12060779, 2021.

Soo, J.-C., Monaghan, K., Lee, T., Kashon, M., and Harper, M.: Air sampling filtration media: Collection efficiency for respirable size-selective sampling, Aerosol Sci. Tech., 50, 76–87, https://doi.org/10.1080/02786826.2015.1128525, 2016.

Spurny, K. R. and Lodge, J. P.: Collection Efficiency Tables for Membrane Filters Used in the Sampling and Analysis of Aerosols and Hydrosols, Tech. Rep. NCAR/TN-77+STR, University Corporation for Atmospheric Research, https://doi.org/10.5065/D6F769JJ, 1972.

Stan, C. A., Schneider, G. F., Shevkoplyas, S. S., Hashimoto, M., Ibanescu, M., Wiley, B. J., and Whitesides, G. M.: A microfluidic apparatus for the study of ice nucleation in supercooled water drops, Lab Chip, 9, 2293–2305, https://doi.org/10.1039/B906198C, 2009.

Stetzer, O., Baschek, B., Lüönd, F., and Lohmann, U.: The Zurich Ice Nucleation Chamber (ZINC) – A new instrument to investigate atmospheric ice nucleation, Aerosol Sci. Tech., 42, 64–74, 2008.

Stopelli, E., Conen, F., Morris, C. E., Herrmann, E., Bukowiecki, N., and Alewell, C.: Ice nucleation active particles are efficiently removed by precipitating clouds, Sci. Rep., 5, 16433, https://doi.org/10.1038/srep16433, 2015.

Sze, K. C. H., Wex, H., Hartmann, M., Skov, H., Massling, A., Villanueva, D., and Stratmann, F.: Ice-nucleating particles in northern Greenland: annual cycles, biological contribution and parameterizations, Atmos. Chem. Phys., 23, 4741–4761, https://doi.org/10.5194/acp-23-4741-2023, 2023.

Tarn, M. D., Sikora, S. N. F., Porter, G. C. E., O'Sullivan, D., Adams, M., Whale, T. F., Harrison, A. D., Vergara-Temprado, J., Wilson, T. W., Shim, J. U., and Murray, B. J.: The study of atmospheric ice-nucleating particles via microfluidically generated droplets, Microfluid. Nanofluid., 22, 52, https://doi.org/10.1007/s10404-018-2069-x, 2018.

Tatzelt, C., Henning, S., Welti, A., Baccarini, A., Hartmann, M., Gysel-Beer, M., van Pinxteren, M., Modini, R. L., Schmale, J., and Stratmann, F.: Circum-Antarctic abundance and properties of CCN and INPs, Atmos. Chem. Phys., 22, 9721–9745, https://doi.org/10.5194/acp-22-9721-2022, 2022.

Testa, B., Hill, T. C. J., Marsden, N. A., Barry, K. R., Hume, C. C., Bian, Q., Uetake, J., Hare, H., Perkins, R. J., Möhler, O., Kreidenweis, S. M., and DeMott, P. J.: Ice Nucleating Particle Connections to Regional Argentinian Land Surface Emissions and Weather During the Cloud, Aerosol, and Complex Terrain Interactions Experiment, J. Geophys. Res.-Atmos., 126, e2021JD035186, https://doi.org/10.1029/2021JD035186, 2021.

Tobo, Y., Adachi, K., DeMott, P. J., Hill, T. C. J., Hamilton, D. S., Mahowald, N. M., Nagatsuka, N., Ohata, S., Uetake, J., Kondo, Y., and Koike, M.: Glacially sourced dust as a potentially significant source of ice nucleating particles, Nat. Geosci., 12, 253–258, https://doi.org/10.1038/s41561-019-0314-x, 2019.

Turner, M., Arellano, F., and Kozloff, L.: Three separate classes of bacterial ice nucleation structures, J. Bacteriol., 172, 2521–2526, 1990.

Twohy, C. H. and Poellot, M. R.: Chemical characteristics of ice residual nuclei in anvil cirrus clouds: evidence for homogeneous and heterogeneous ice formation, Atmos. Chem. Phys., 5, 2289–2297, https://doi.org/10.5194/acp-5-2289-2005, 2005.

Vali, G.: Quantitative evaluation of experimental results on the heterogeneous freezing nucleation of supercooled liquids, J. Atmos. Sci., 28, 402–409, 1971.

Varble, A. C., Nesbitt, S. W., Salio, P., Hardin, J. C., Bharadwaj, N., Borque, P., DeMott, P. J., Feng, Z., Hill, T. C. J., Marquis, J. N., Matthews, A., Mei, F., Öktem, R., Castro, V., Goldberger, L., Hunzinger, A., Barry, K. R., Kreidenweis, S. M., McFarquhar, G. M., McMurdie, L. A., Pekour, M., Powers, H., Romps, D. M., Saulo, C., Schmid, B., Tomlinson, J. M., van den Heever, S. C., Zelenyuk, A., Zhang, Z., and Zipser, E. J.: Utilizing a Storm-Generating Hotspot to Study Convective Cloud Transitions: The CACTI Experiment, B. Am. Meteorol. Soc., 102, E1597–E1620, https://doi.org/10.1175/BAMS-D-20-0030.1, 2021.

Vergara-Temprado, J., Miltenberger, A. K., Furtado, K., Grosvenor, D. P., Shipway, B. J., Hill, A. A., Wilkinson, J. M., Field, P. R., Murray, B. J., and Carslaw, K. S.: Strong control of Southern Ocean cloud reflectivity by ice-nucleating particles, P. Natl. Acad. Sci. USA, 115, 2687–2692, 2018.

von der Weiden, S.-L., Drewnick, F., and Borrmann, S.: Particle Loss Calculator – a new software tool for the assessment of the performance of aerosol inlet systems, Atmos. Meas. Tech., 2, 479–494, https://doi.org/10.5194/amt-2-479-2009, 2009.

Welti, A., Müller, K., Fleming, Z. L., and Stratmann, F.: Concentration and variability of ice nuclei in the subtropical maritime boundary layer, Atmos. Chem. Phys., 18, 5307–5320, https://doi.org/10.5194/acp-18-5307-2018, 2018.

Wex, H., Augustin-Bauditz, S., Boose, Y., Budke, C., Curtius, J., Diehl, K., Dreyer, A., Frank, F., Hartmann, S., Hiranuma, N., Jantsch, E., Kanji, Z. A., Kiselev, A., Koop, T., Möhler, O., Niedermeier, D., Nillius, B., Rösch, M., Rose, D., Schmidt, C., Steinke, I., and Stratmann, F.: Intercomparing different devices for the investigation of ice nucleating particles using Snomax® as test substance, Atmos. Chem. Phys., 15, 1463–1485, https://doi.org/10.5194/acp-15-1463-2015, 2015.

Whale, T. F., Murray, B. J., O'Sullivan, D., Wilson, T. W., Umo, N. S., Baustian, K. J., Atkinson, J. D., Workneh, D. A., and Morris, G. J.: A technique for quantifying heterogeneous ice nucleation in microlitre supercooled water droplets, Atmos. Meas. Tech., 8, 2437–2447, https://doi.org/10.5194/amt-8-2437-2015, 2015.

Wilson, T. W., Ladino, L. A., Alpert, P. A., Breckels, M. N., Brooks, I. M., Browse, J., Burrows, S. M., Carslaw, K. S., Huffman, J. A., Judd, C., Kilthau, W. P., Mason, R. H., McFiggans, G., Miller, L. A., Nájera, J. J., Polishchuk, E., S. Rae, C. L. S., Si, M., Temprado, J. V., Whale, T. F., Wong, J. P. S., Wurl, O., Yakobi-Hancock, J. D., Abbatt, J. P. D., Aller, J. Y., Bertram, A. K., Knopf, D. A., and Murray, B. J.: A marine biogenic source of atmospheric ice-nucleating particles, Nature, 525, 234–238, 2015.

Wright, T. P. and Petters, M. D.: The role of time in heterogeneous freezing nucleation, J. Geophys. Res.-Atmos., 118, 3731–3743, 2013.

Yankovsky, S. A., Levin, Z., Berthold, T., and Sandlerman, N.: Some basic characteristics of bacterial freezing nuclei, J. Appl. Meteorol., 20, 1013–1019, 1981.

Zíková, N., Ondráček, J., and Ždímal, V.: Size-Resolved Penetration Through High-Efficiency Filter Media Typically Used for Aerosol Sampling, Aerosol Sci. Tech., 49, 239–249, https://doi.org/10.1080/02786826.2015.1020997, 2015.